Synthesis and Characterization of TiB_2 Nanosheets, and Application as Photocatalyst

By

Sairah Qayyum

School of Chemical and Materials Engineering

National University of Sciences and Technology

2021

Synthesis and Characterization of TiB_2 Nanosheets, and Application as Photocatalyst

Name: Sairah Qayyum

Registration. No: 00000204575

This thesis is submitted as partial fulfillment of the requirements for the degree of

MS in Nanoscience and Engineering

Supervisor Name: Dr. Sofia Javed

School of Chemical and Materials Engineering (SCME)

National University of Sciences and Technology (NUST)

H-12 Islamabad, Pakistan

August, 2021

Dedication

“I dedicate this thesis to my beloved parents.”

Acknowledgments

Allah Almighty is the One, who bestows and gives the power to us to think, utilize our expertise in knowledge in achieving remarkable solutions for mankind in every field. Therefore, I express my greatest thanks to Almighty Allah the universal and the architect of the world, who has gifted us the brain and unstable nature construction of knowledge and body to achieve our work in the form of this project report.

I like to express my gratefulness to supervisors Dr. Sofia Javed, my GEC Members Dr. Aftab Akram, and Dr. Rahim Jan for their clear and patient guidance that directed me to fulfill my project. Their valuable suggestions and feedback contributed greatly to this thesis.

I am thankful to all the faculty members to build my basis of Nanoscience and Engineering. I want to thank Ms. Kanza Iqbal, Ms. Maham Iqra, Ms. Sidra tul Muntha, Ms. Amna Hussain and Mr. M Tayyab Ahsan for their continuous support and motivation which helped me at various stages during my Masters.

I acknowledge the support provided by the Materials Engineering Department of SCME for providing me a platform to perform to utilize my skills in research work.

I acknowledge the financial aid and technical assistance provided by our department, SCME, during my research experience and made this project work memorable forever. Last, but not the least, I want to thank my family for their prayers, support, and confidence in me without which I would not have been able to reach my full potential.

-Sairah Qayyum

Abstract

The evolution of nanotechnology in the past few decades has provided enormous opportunities and scope to mitigate polluted water by using nanomaterials created with specific properties. Titanium diboride (TiB_2), an emerging two-dimensional (2D) nanosheets possess a unique combination of chemical and physical properties. It is a low-density, ultra-high temperature refractory material that has gained importance in recent years. In this research, 2D nanosheets of TiB_2 were synthesized by liquid exfoliation method, characterized by XRD, UV-visible spectroscopy, SEM, and AFM techniques. Synthetic dyes are significant component of our lives as they are found in the various industrial products forming significant constituent of industrial wastewater. Dye degradation is a method in which the synthetic dye molecules are chemically broken down into smaller molecules resulting into non-toxic products. Titanium diboride has good electrical properties. Being a UV absorbing material, with a slightly larger Eg, it can reduce charge recombination rate and enhance photocatalytic activity. Another nanomaterial titanium dioxide (TiO_2) has been used widely for notable applications like refinement of polluted water & air, self- cleaning glasses, tiles, and tents. Exfoliated nanosheets and TiO_2 nanoparticles were used to prepare TiB_2@ TiO_2 nanocomposite with 0.5%, 1%, and 2% of nanosheets. The prepared composite samples were used for photocatalytic degradation of Rhodamine B dye. The composite degraded more than 50 % of Rhodamine B in 90 minutes only under UV illumination.

Table of Contents

List of Figures

List of Tables

List. Of. Abbreviations

TMDC.....Transition metal dichalcogenide

TMD….....Transition metal diborides

GNSs….....Graphene nanosheets

NPs….....Nanoparticles

CB.....Conduction Band

Chapter 1

Introduction

Environmental pollution has become a prolonged global dilemma due to the accelerated pace of urbanization and massive industrialization. Although substantial efforts have been employed on the removal and degradation of dangerous environmental contaminants, environmental remediation is yet a matter of global interest. The evolution of nanotechnology over the past few decades has provided enormous opportunities and scope to mitigate polluted water by using nanomaterials created with specific properties. [1]

The main contributors to water pollution are the textile, and dye manufacturing industries. According to an estimate, 17% - 20% of industrial water pollution is the result of textile pigmentation and treatment processes globally. The discharge of such untreated wastes into the water channels is resulting in the extinction of aquatic life and agitation in the ecological balance. It also leads to many diseases and health complications in human beings. Degradation of these water pollutants by employing light-absorbing materials under the solar spectrum is a highly efficient, and economical approach for the treatment of wastewater. Photocatalysis provides an easy way to remove the toxic organic dyes present in wastewater using solar radiation. [2][3]

As **Richard P. Feynman said "There is plenty of room at the bottom."** and presented us "an invitation to enter a new field of physics" in 1959. [4][5]

At that time, he categorized "the problem of manipulating and controlling things in a small scale" into 10 questions on writing technique, information storage, high resolution microscopy, biological system, miniaturization of computing and manufacturing, lubrication, micro- processing, atom rearrangement, and chemical synthesis. Since then, more than two decades it took, for nanotechnology to arrive at its booming era in late 80's. Renowned discovery of buckminsterfullerene and various fullerenes by Nobel laureates Dr. Richard E. Smalley, Dr. Robert F. Curl, and Dr. Harold W. Kroto in 1985 sparked off the enthusiasm of nanoscience research. Soon after the discovery of carbon nanotubes in 1991 same year, the first

nanotechnology program was established by the National Scientific Fund in US. [5][6]

Nanotechnology and nanomaterials grant possibilities for the generation of truly distinct materials in terms of dimensions and properties from their bulk counterparts.

1. Zero Dimensional (0D) Nanostructures

Zero dimensional nanomaterials have a diameter of less than 100 nm, with spherical or quasi- spherical shape. Because of their intrinsic structural properties such as high surface-to-volume ratios, the quantum and edge confinement effects and the ultra-small size providing more refined or unique properties e.g. quantum efficiency, high photoluminescence, and chemiluminescence. Carbon quantum dots (CQDs), graphene quantum dots (GQDs), fullerenes, inorganic quantum dots, magnetic nanoparticles, noble metal nanoparticles, have drawn inclusive research interest in the areas of ion detection, biosensing, biomolecular recognition, disease diagnosis and athogen detection. [8][9]

Titanium dioxide is being investigated for many decades, titania nanoparticles have been studied for dye-sensitized solar cells, humidity sensors, photocatalysts, and in medicine for treatment of maladies and cancer. [9][10][11]

TiO_2 nanoparticles doped with nitrogen loaded on magnetic hexagonal mesoporous silica for removal of herbicides are shown in fig 1.1. [10]

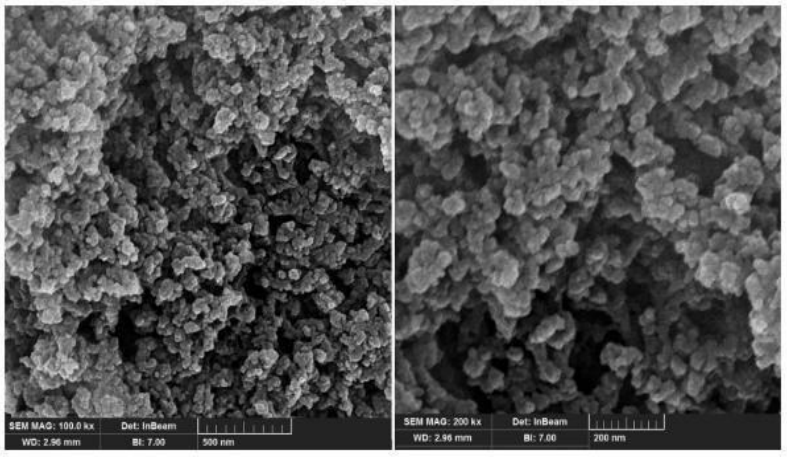

Fig. 1.1 SEM image of TiO_2 nanoparticles [10]

Titanium diboride nanoparticles have excellent properties like good tensile strength, ductility, super hardness, and yield strength and corrosion susceptibility. [12][13]

Nanocrystalline titanium diboride particles were synthesized with a novel approach having 15-40 nm average diameter and hexagonal crystal structure. TEM image of these nanoparticles as shown in fig. 1.2. [14]

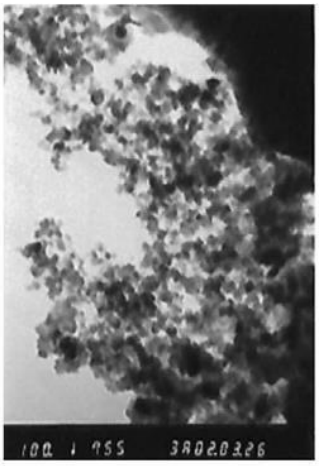

Fig 1.2. TEM image of TiO_2 nanoparticles [14]

A scalable synthesis route of TiB_2 nanoparticles was reported by Javadi et al. with particle size of less than 10 nm. The characterization of the sample confirmed the synthesis of surface-clean, ultra- fine TiB_2 nanoparticles (shown in fig 1.3). [15]

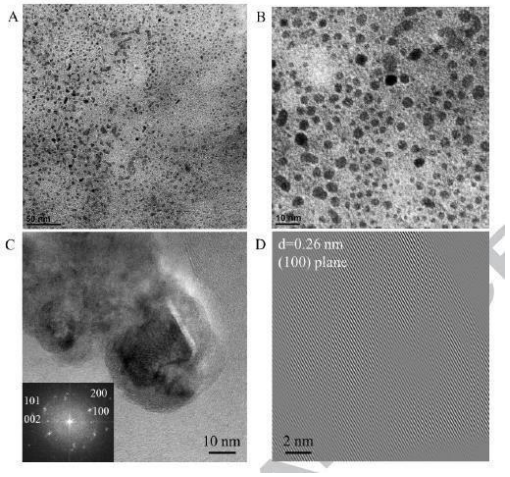

Fig. 1.3 TEM images of TiB_2 nanoparticles [15]

Alumina-titanium diboride nanocomposite formed by a sol-gel route followed by mechano- chemical reduction. The results shown (fig 1.4) that in the Al2O3 matrix, 10- 30 nm-sized TiB_2 particles were dispersed. This low-temperature process successfully produced homogenous composite powder of 100 nm – 2 μm sized particles. [16]

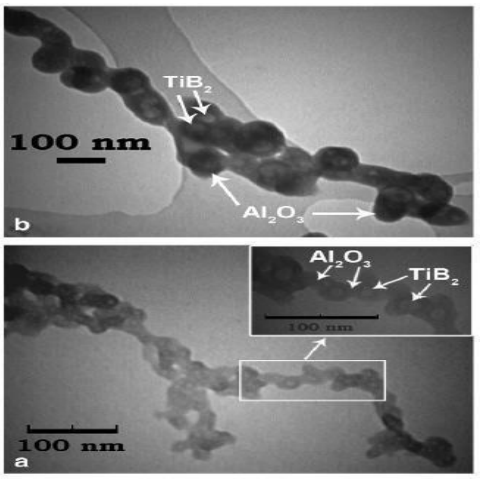

Fig. 1.4 TEM images of alumina-titanium diboride nanocomposite [16]

1.2 One Dimensional (1D) Nanostructures

1D nanostructures is with lateral dimensions between 1-100 nm include nanowire, nanorods and nanotubes. They are suitable model for quantum confined physics research. Unique electrical and thermal transport, mechanical properties make 1D nanostructures promising candidates in applications such as electronics, optoelectronic and electromechanical devices. [17]

Popular fabrication methods include templated deposition, self-assembly, lithography, chemical methods (e.g., chemical vapor deposition for carbon nanotubes) and their combinations. Using chemical method, nucleation and growth are the two main processes for the crystallization of 1D structures. The anisotropic in crystal structure and chemical bonding is the major driven force of one-dimensional growth of the materials. [18] Many 1D nanostructures have been explored for their

potential in various applications. Besides the first discovered carbon nanotubes (CNTs), another remarkable example is TiO_2 1D structures such as nanowires, nanorods and nanobelts, or their optic and electronic properties. Potential applications of TiO_2 1D nanostructures include solar cell, photocatalysis, ion-intercalation batteries and sensors. [11][10][19]

A simple hydrothermal method is used for the successful synthesis of TiO_2/TiB_2 nanowall (fig 1.5). The results showed photocatalytic performance of A- TiO_2/TiB_2 catalysts is better than P-25 TiO_2 because of the decolorization rate of A- TiO_2/TiB_2 is 78.8% after 180 min in MB solution. The absorption edge of A- TiO_2/TiB_2 catalyst and broadening absorption peak has shifted to low energy systems. Further characterization of the sample indicated this peak shifting was due to N- doping in TiO_2/TiB_2 nanowall. [20]

Another 1D TiO_2/TiB_2 hybrid material was formed via a facile solvothermal route with varying morphologies.

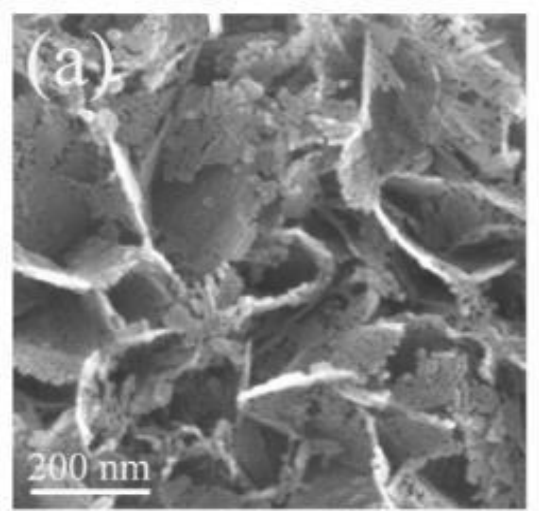

Fig 1.5. SEM image of TiO_2/TiB_2 nanowall [20]

1.3 Two Dimensional (2D) Nanostructures

2D nanomaterials have charge confinement in one dimension and mobile in the remaining two spatial dimensions. These 2D materials possess novel and superior properties distinct from their bulk counterparts. In the last two decades research on 2-

D materials has drawn enormous attention since the successful exfoliation of graphite into atomically thin 2-D graphene in 2004. Graphene has extraordinary properties including lightweight, strength, flexibility, and high optical transmittance. [22]

This “wonder material” of the 21st century can be employed for ultra-wide-bandwidth optical modulators, faster transistors, and many other applications. Another group of layered materials is known as transition metal dichalcogenides (TMDCs). These layered materials have van der Waals bonding, and hexagonal structure, enabling the exfoliation of the materials into 2D flakes with atomic-level thickness. [23]

From the layered materials family of transition metal diborides, TiB_2 stable 2D nanosheets in aqueous dispersions by first successful exfoliation of bulk polycrystalline TiB_2 with high boron- to-titanium ratio.

This process requires repeated cycles of turbulence-assisted shear exfoliation and ultrasonication of TiB_2 bulk powder in aqueous medium. AFM results showed (fig.1.6) nanosheets of 6–10 nm thickness and TEM revealed several microns sized sheets. [24]

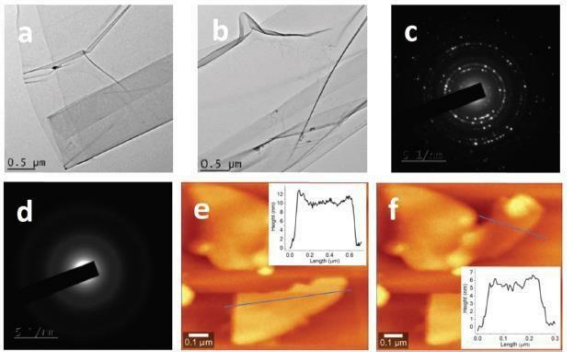

Fig 1.6 AFM and TEM images of TiB_2 nanosheets [24]

The borothermal reduction of TiO_2 with the assistance of $MgCl_2$ at low temperature and flowing argon atmosphere led to the successful synthesis of TiB_2 nanosheets K. -H. Wu et al. reported. The formation mechanism of TiB_2 nanosheets consists of the dissolution-recrystallization

mechanism and the co-effects of $MgCl_2$ and B_2O_3. The nanosheets had a lamellar structure (fig. 1.7) and specific surface area of 99.32 m^2/g after a 4 h reaction of an

$MgCl_2$ and TiO_2 at 1373 K. [25]

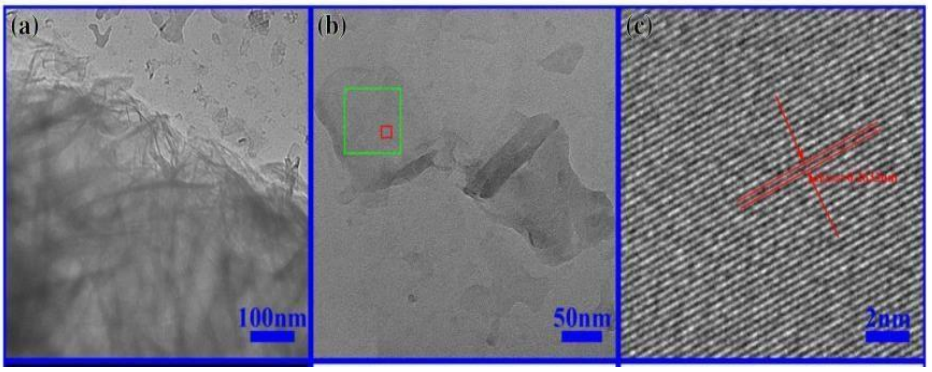

Fig 1.7. TEM images of TiB_2 nanosheets [25]

Epitaxial, low-resistivity, and smooth titanium diboride films on SiC substrates. The films grown by pulsed-laser deposition technique have resistivity comparable to that of single-crystal TiB_2 and the structural and chemical affinity of material and lattice match is comparable to the superconductor MgB_2. The growth of TiB_2 films (fig1.8) is a big step towards MgB_2-based heterostructures. The electrical resistivity of the epitaxial TiB_2 films measured at 300 K is 8 mΩcm. [26]

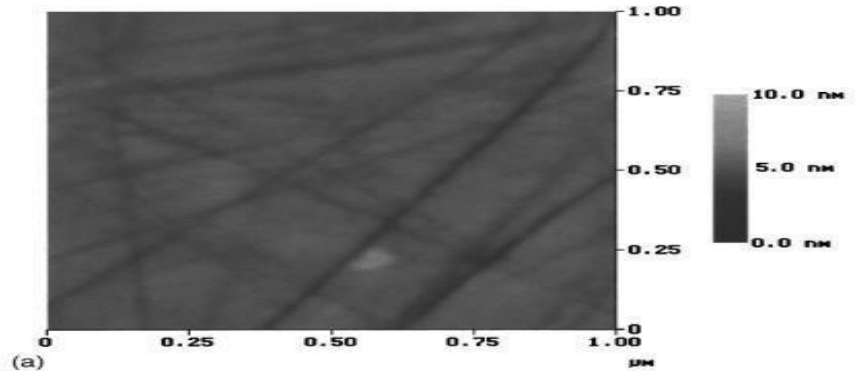

Fig 1.8. AFM Surface morphology of TiB_2 film [18]

Highly photoactive, slit shaped two-dimensional titanium dioxide nanostructures shown in fig.1.10. These 2D nanostructures were synthesized without any environmentally dangerous materials or organic solvents. [27]

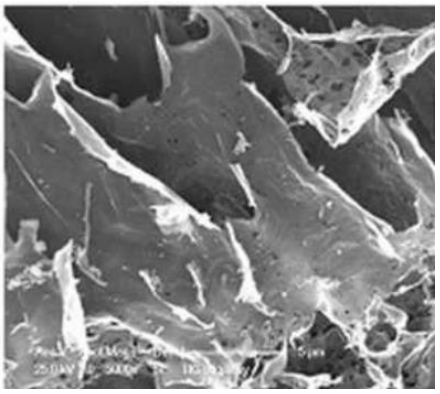

Fig 1.9. SEM images of 2D TiO_2 nanostructures [27]

1.4 Three Dimensional (3D) Nanostructures

Three-dimensional materials possess three arbitrary di-mensions surpassing the nanoscale (>100 nm). Yet, 3D materials maintain a nanocrystalline structure or include the occupancy of traits at the nanoscale. They are constituted by recurring patterns of nanosize crystals, usually in diverse orientations. These include bulk structures such as carbon nanobuds, which incorporates CNTs and fullerenes, aerogels, fuller-ites, honeycombs, fibers, hydrogels, and foams for the fabrication of additive- and binder-free electrodes, conductive for supercapacitors.[8][28]

TiB_2-TiC/TiO_2 porous heterostructures having improved surface area and photocatalytic performance were synthesized by the hydrothermal route. The TiB_2-TiC/TiO_2 heterostructures (fig.1.10) have TiO_2 nanobelts and nanosheets which have shown improved photocatalytic degradation of rhodamine B and methyl orange. [29]

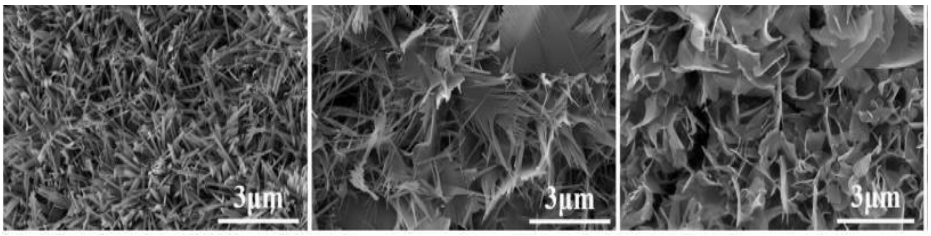

Fig. 1.10 SEM: TiB_2-TiC/TiO_2 nanosheet heterostructure [29]

A three-dimensional Ag-titanium dioxide nanowires structure shown in fig 1.11, with surface enhanced Raman scattering, recyclability, and excellent performance for detection of biological and chemical molecules. [30]

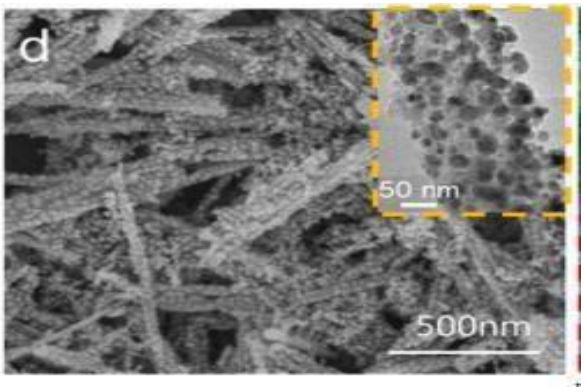

Fig 1.11 SEM and TEM images of TiO_2 NWs and Ag-TiO_2 NW [30]

Titanium dioxide embed carbon nanofibers hybrid 3D composites was formed to enhance electrochemical performance of sulfur cathode in batteries.

The fig. 1.12 shows SEM images of mesoporous 3D titanium dioxide embed carbon nanofibers/S. [19]

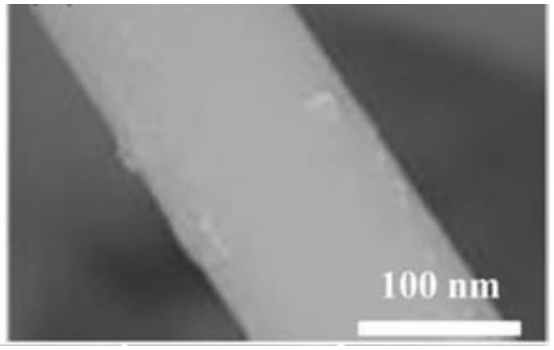

Fig.1.12 SEM image of the CNFs@TO composites [19]

1.5 TiO_2 and Photocatalysis

Numerous diverse nanotechnology-based methods for the treatment of wastewater have been developed. The most generally applied techniques are photocatalytic water treatment technology, membrane-based technology, sensing and monitoring technology, adsorption-based technology, and anti-microbial nanomaterials-based technology. TiO_2 is an accepted and the most studied practical material in semiconductor photocatalysis. [33]

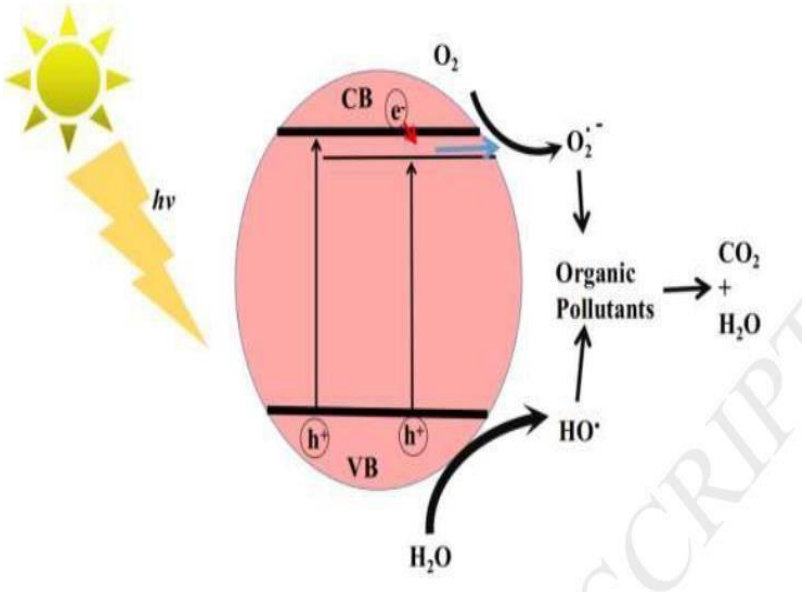

Fig1.14 Schematics of Photocatalytic mechanism [33]

For the degradation of different lethal pollutants in water and air, TiO_2 nanoparticles have been largely employed. Despite owning diverse benefits, such as abundant and cheap, nontoxicity, strong oxidizing power, high stability, and the superior photoelectric effect, the wide bandgap energy (3.2 eV) of TiO_2 aids the requirement of using ultraviolet (UV) excitation to achieve applications. The TiO_2 catalyst also encounters deactivation when its continuously utilized for VOC degradation. A suitable approach for narrowing the bandgap of TiO_2 is needed to utilize maximum photons from the solar spectrum. [34][35][36]

Nano Mg Fe– TiO_2 photocatalyst was synthesized with doping of Mg and Fe into TiO_2, for visible light photocatalysis. They help in preventing the recombination of electrons and holes during the reaction. The catalyst showed better removal efficiency for Congo Red Dyes as compared to TiO_2. [37]

For the degradation of methyl orange (MO), TiO_2 /WS_2 composite photocatalyst was utilized, which showed excellent degradation efficiency. The catalyst successfully degraded ~95% of methyl orange in 60 mins under a 500W Xenon lamp. [38]

Methylene blue was degraded using thulium doped TiO_2 composite material. Two crystalline phases allowed better efficiency of the charge separation, and the pyrochlore phase enhanced the mobility of the photogenerated electrons. [39]

Visible light degradation of Rhodamine-B using Erbium-doped mesoporous TiO_2 catalyst was analyzed, which showed 98.78 % degradation of Rhodamine-B in 28 min. The large surface area of mesoporous TiO_2 structure, improved O_2 adsorption by Erbium, and photostability of the catalyst make it suitable for industrial wastewater treatment under visible light illumination. [33] Titania co-doped with iron (0.5 wt%) and nitrogen under visible-light irradiation decomposed Rhodamine B completely within 4 hours. The efficiency of this composite is far better than Fe-doped TiO_2 or N-doped TiO_2. [40]

Catalyst with greater surface area offer higher photocatalytic activity. In the next section, we will discuss Titanium Diboride a layered material from transitional metal diborides family as potential material for developing photocatalyst**.**

1.6 Transitional Metal Diborides

Transition metal dichalcogenide (TMDC) monolayers, such as molybdenum disulfide and diselenide, tungsten disulfide and diselenide, have drawn attention from material scientists. However, there is one group of interesting materials that has been overlooked in the field of nanoscale research – transition metal diborides. Transition metal diborides consist of group IV- VII transition metals (TM= Ti, Zr, Al, V, Ti, Cr, Nb, Zr, Ta, and Mo, etc) also known as 3d, 4d, and 5d TMB_2. They have been under investigation due to their outstanding properties like increased hardness, high melting

point & thermal conductivity, wear resistance, enhanced strength and chemical stability. Transition metal diborides, having both metallic and ceramics, properties fall in the category of ultrahigh temperature ceramics. [23][24]

For ultra-high temperature applications like cutting tools, rocket nozzles, electrodes, wear resistant parts and armor, TaB_2, TiB_2, ZrB_2, and HfB_2 (refractory borides) are promising candidates due to their melting temperatures up to approx. 4000 °C and superior chemical and thermomechanical properties. [25][29] Their superior properties at elevated temperatures make them a potential candidate for manufacturing parts like nose tips, hot structure components of hypersonic vehicles, scramjet engines and microelectronics. [41][42]

The table 1 includes values for different properties of TMBs.

Table1: General trend in the properties of TMBs

Property	Values for TMBs
Thermal conductivity	60 W/mK to 120 W/mK
Density	4.5 g/cc - to 12.5 g/cc
Hardness	25 GPa to 35 GPa
Electrical resistivity	9 μΩ.cm - 33 μΩ.cm
Thermal expansion co-efficient	6.3×10^{-6} K^{-1} to 8.6×10^{-6} K^{-1}
Fracture toughness	4 $MPam^{1/2}$ to 5 $MPam^{1/2}$

Reference: **[**29][41][42][43][44]

Metal diborides form a huge family of at least 30 members of the periodic table. Most of them have an AlB_2-type hexagonal structure, having boron layers exactly like graphitic layers. The boron atoms are joined through covalent bonding in 3D metal diboride structures. The boron layers provide high electrical conductivity in these diborides. The arrangement of boron atoms affects the chemical and physical properties. Metal diborides have attracted researchers since the discovery of

magnesium diboride as a superconductive material at 39 K. [43][44]

Among transition metal diborides, Titanium diboride (TiB_2), for example, an industrial ultra-hard ceramic possesses properties like hardness, chemical resistance, oxidation resistance and high conductivity both thermally and electrically. [45]
By creating nanoscale structures of titanium boride compounds, we can extend these advantages to nanoscale devices and products, for instance, electrodes, aircraft materials, durable electronics, and heterostructures incorporating other nanomaterials. [16][46]

Boron rich ceramics have always been of interest to industrial research, since the 60s, for their remarkable mechanical performance, possible superconductivity and antiferromagnetism. Commonly appreciated are metal diborides, with crystal structures of hexagonal B atomic planes intercalated by close-packed metal atom layers. Metal atoms donate electrons to B-B covalent bonds. Typical covalent bonds between B atoms observed in metal diborides have the same length of B-B single bond, varying between 1.7 to 1.8 Å. The metal-B bond is predominantly covalent, as well, confirmed by both theoretical calculation and experimental observation.
Like many metal nitrides and carbides ceramic materials, borides have durable mechanical performance of high hardness, wear-resistance and melting point, for applications in hard composites like crucibles, armors, and wear-resistant coating. Metal diborides also have high electronic conductivity, thus, considered to be potential diffusion barriers and nanowires in electronics. [47][48][49][50] TiO_2 in composition with layered TiB_2 will provide an enhanced surface area which acts as an active reaction site for photocatalysis and better separation of charge carriers.

1.6.1. Lattice Structure of TiB_2

AlB_2 type structure was first published in the 1930s with 191 PG/mmm, space group, containing boron layers separated by layers of metals in a hexagonal close-packed structure. [51] The hexagonal boron rings are stacked above and below metal atoms perpendicular to the c axis as shown in Fig. 1.15 and Fig. 1.16. [52] [53][54]

Among transition metal diborides, Titanium diboride holds a special position because

of its excellent electrical resistivity of 22 x10^6 Ω cm, high melting point i.e. 3225ºC, increased hardness of 25 GPa, low density of 4.5 g/cm^3, chemical stability at high temperatures and better thermal conductivity of 96 W/m/K.

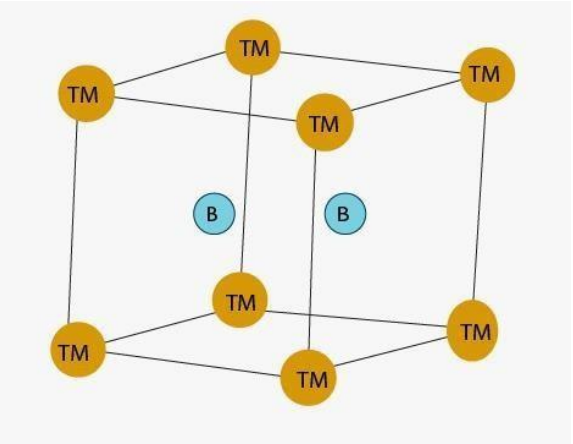

Fig. 1.15 Unit cell of TiB_2

These properties make TiB_2 a potential material for cutting tools, arms, wear, erosion resistance, crucibles, high-temperature electrode, microelectronics, mechanical components, and high-temperature structural applications.[55][56]

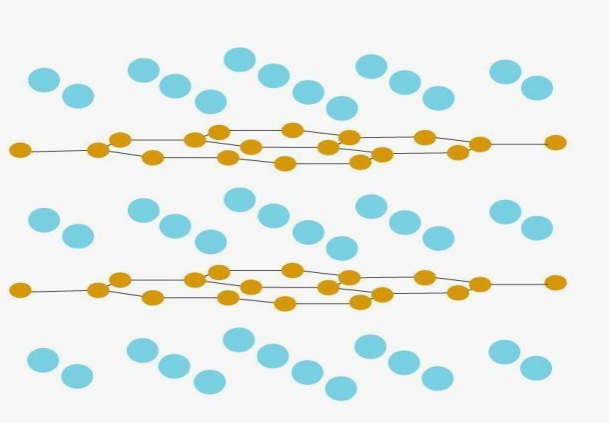

Fig.1.16 AlB_2 type layered transition metal diborides structure; Blue- Boron, Orange – TM

The theoretical and experimental values of lattice parameters of TiB_2 crystal structure are represented in the table 1.

Table 2: Theoretical and experimental lattice parameters of TiB_2

TMD2	a Å			c Å		
TiB_2 Experimental	3.006 [a]	3.03 [b]	3.032 [C]	3.212 [a]	3.22 [b]	3.229 [c]
TiB_2 Theoretical	3.005 [a]	3.038 [a]	3.070 [a]	3.186 [a]	3.239 [a]	3.262 [a]
	3.03 [b]	3.034 [d]	3.030 [e]	3.23 [b]	3.226 [d]	3.221 [e]

References: a [55], b [57], c [58], d [59], e [24]

1.6.2. TiB_2 Properties

TiB_2, for its unique properties and diverse applications, draws interest to the fabrication and characterization. However, there is no current standard procedure for high quality TiB_2 production, leading to severe variation in chemical composition and performance of the products. The data presented above have confirmed the strong dependence of properties on microstructure. Overall, the exquisite performance of TiB_2 can be summarized as in table 3.

Table: 3 Properties of polycrystalline TiB_2

	Temperature (°C)					
Property	**20**	**500**	**1000**	**1200**	**1500**	**2000**
Density (g/cm^3)	4.500	4.449	4.389	4.363	4.322	4.248
Thermal Conductivity (W/(m·K))	96	81	78.1	77.8		
Compressive Strength (GPa)	1.8					
Hardness (GPa)	25	11	4.6			
Bulk Modulus (GPa)	240	234	228			
Fracture toughness (MPa.$m^{1/2}$)	6.2					
Elastic Modulus (GPa)	565	550	228			
Wear Coefficient (10^{-3})	1.7					
Electrical conductivity	$0.45x\ 10^{-6}$					

Reference: [56][59]

Chapter 2

Literature review

In the field of nanomaterials, two-dimensional nanomaterials show immense potential and applications due to their unique physicochemical properties. In the recent past, researchers are making efforts to exfoliate layered materials including transition metal diborides. Bulk titanium diboride has been used in numerous industrial applications for decades, while continuous efforts to delaminate it into 2D nanosheets have provided new prospects and applications.

Saju K. John et al. reported high boron-to-titanium ratio TiB_2 stable 2D nanosheets in aqueous dispersions by first successful exfoliation of bulk polycrystalline TiB2. This process requires repeated cycles of turbulence-assisted shear exfoliation and ultrasonication of TiB_2 bulk powder in aqueous medium. [24]

F. Huang et al. used a simple hydrothermal method for the successful synthesis of TiO_2/TiB_2 nanowall. This route required ethylenediamine (EDA) and hydrogen peroxide solution, the addition of EDA initiated the arrangement of layered products to A-TiO_2/TiB_2 core/shell nanowall structure. The results showed photocatalytic performance of A-TiO_2/TiB_2 catalysts is better than P-25 TiO_2 because of the decolorization rate of A-TiO_2/TiB_2 is 78.8% after 180 min in MB solution. The absorption edge of A-TiO_2/TiB_2 catalyst and broadening absorption peak has shifted to low energy systems. Further characterization of the sample indicated this peak shifting was due to N-doping in TiO_2/TiB_2 nanowall. [20]

A. Yousaf et al. reported the synthesis of 2D nanosheets of metal diborides including AlB_2, CrB_2, HfB_2, NbB_2, MgB_2, TiB_2, TaB_2, and ZrB_2, via ultrasonication-assisted exfoliation. Tip sonication and bath sonication methods were used for exfoliation and each metal diboride powder was mixed with a suitable organic solvent or aqueous surfactant solution to make dispersions e.g sodium cholate (SC) aqueous solution for TiB2. The lateral dimension of exfoliated sheets has a length up to micrometers and thickness down to 2-3 nm. The exfoliated metal diboride layers retained their

chemical composition and hexagonal structure with a lateral dimension up to micrometers and thickness down to 2-3 nm. TEM results showed the size of flakes varying from 100 nm across to several microns across and morphologies like flat, planar sheets for Mg, Al, Ti, and Cr diborides and folded, crumpled for Zr, Nb, Hf, and Ta diborides. AFM results showed thicknesses varying between 3 to 18 nm and lateral dimensions from 150 nm to 4 μm across. [60]

X. Guo et al. synthesized TiB_2-TiC/TiO_2 porous heterostructures having improved surface area and photocatalytic performance. The hydrothermal route was used to achieve in situ growth of porous structure with boron and carbon elements. The TiB_2-TiC/TiO_2 heterostructures have TiO_2 nanobelts and nanosheets which have shown improved photocatalytic degradation of methyl orange and rhodamine B as compared to pure porous TiB_2-TiC composite. [29]

The table below briefly describes research on TiB_2 with applications in diverse fields.

Table: 4 TiB_2 structures, composites, and Applications of TiB_2

Material	Method	Size	Properties	Application	Reference
Zn-TiB_2 Nanocomposite	Flux-assisted synthesis, hot rolling and ultrasound-assisted nanoparticle homogenization	Size: 454nm	Improved Yield stress by 90% and ultimate tensile stress by 45%	biodegradable material for load-bearing applications	[62]
$MgNi_3B_2$ and TiB_2 Nanoparticl-es	Sol-gel and ball milling	TiB_2 species approx. 5 nm	hydrogen desorption kinetics of Li-Mg-B- H RHC was massively affected	Li-Mg-B-H is excellent cyclic stable hydrogen storage system	[63]
Die-cast AlSiMgCu/ TiB_2 composite	High Pressure Diecasting assisted with Super vacuum	TiB_2 particles	Superb hardness, yield strength, tensile strength and an industrially applicable ductility	Approximately 90% increase in strength compared to traditional alloys ensuring for industrial applications.	[12]
Al_2O_3–TiB_2 nanocomposite films	Atmospheric Plasma spray (APS) technique	Al_2O_3-30 wt% TiB_2 film thickness 30–45 μm.	High hardness and corrosion resistance	Biocompatible films could be used for Orthopedic and dental applications.	[64]

Chapter 3

Experimentation Methods

3.1 Synthesis Routes

For the synthesis of 2D material bottom-up and approaches are used. In this work, top-down approach is used to synthesize titanium diboride nanosheets. The general top-down and bottom- up approaches for 2D materials are discussed below:

3.2 Top-Down Approaches

The preparation of mono or a few layered materials from the exfoliation of 2D materials is one prominent area of importance [61]. Exfoliated structures provide interest both in their potential applications and fundamental investigations. Materials synthesized from exfoliation of graphite, TMDs and, Transition metal diborides have enormous significance as they present a breakthrough in optoelectronics and flexible electronic devices. In 2D nanostructures, weak bonding between their layers and strong in-plane bonding [62] [65] play a vital role so that these layers can be separated from each other to enhance surface area and the inherent properties of materials. Exfoliation can be performed by:

3.2.1 Mechanical exfoliation

In this process, the layers are exfoliated by employing some mechanical forces.[63]

Graphene was successfully synthesized by this process by using bulk graphite by **"scotch tape method"** [64]. Through this approach, high-quality single layers can also be developed. This technique is successful as it generates intrinsic sheets, and a huge domain of research is directed towards it now.

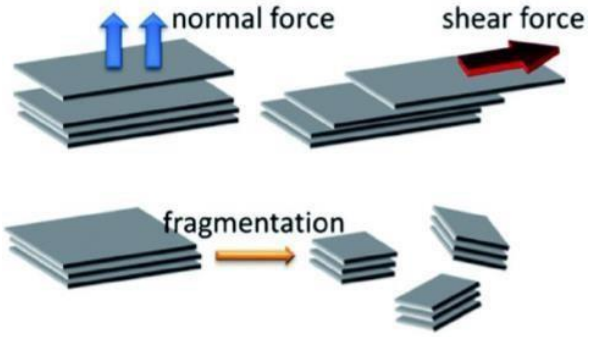

Fig. 3.1 Schematics for mechanical Exfoliation of 2D materials

3.2.1.1 Merits

- Pristine quality sheets are obtained.

3.2.1.2 Demerits

- Limited yield is obtained through this method.
- Lack of scalability [65].
- Not relevant for large-scale results.
- Sheet size and thickness constraining is a problem.

3.2.2 Liquid Phase Exfoliation

In this process, solvents are utilized to intercalate the layers of the material [66]. In the sonication process, sound energy is utilized which produces shear forces. The solvent is a crucial choice, i.e., it needs to promote the delimitation process. It shouldmaintain extremely stabilized dispersions with a high density of 2D exfoliated sheets. Seldom a blend of solvents may also be utilized for effective exfoliation of materials. Among solvents, N- methyl-2-pyrrolidone (NMP) is the most common. NMP has a surface energy of ~40 mJ m-2 which balances with the surface energy of

several layered materials [67][69].

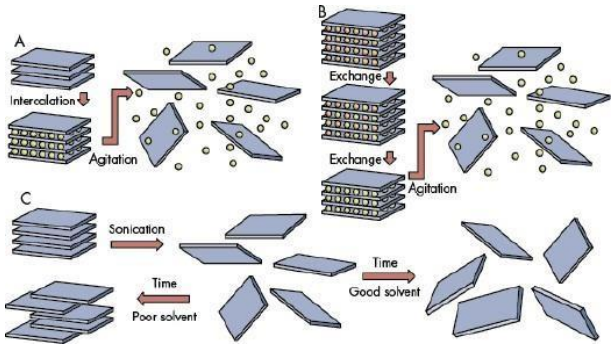

Fig. 3.2 Schematics for liquid phase exfoliation of 2D materials

3.2.2.1 Merits

- High yield can be achieved through this process.
- The extremely crystalline material is produced.
- This process is cost-effective and cost-effective.
- Sheets of reliable scalability are produced.

3.2.2.2 Demerits

- Comprises residual chemicals, which can alter the characteristics of nanosheets.
- The solvent may be unstable and lethal too.
- This approach can provoke defects in 2D structures and decrease flake size to a hundred nanometers.

3.3 Bottom-up approaches

Also, there are many ways to develop 2D materials via bottom-up approaches like:

1. Wet chemical synthesis

2. Chemical vapor deposition [68]

Here, we have used top-down approach to synthesize nanosheets.

3.4 Aims and Objectives

The aim of this study includes:

- Synthesis of TiB_2 nanosheets through liquid exfoliation method.
- Characterization of the synthesized nanosheets.
- Synthesis of TiB_2@TiO_2 nanocomposite for photocatalytic application.

3.5 Synthesis of TiB_2 Nanosheets and TiB_2@TiO_2 Nanocomposite

3.5.1 Synthesis of Exfoliated TiB_2 Nanosheets

To synthesize titanium boride nanosheets liquid exfoliation method was used. Titanium diboride powder was added in N-methyl-2-pyrrolidone (50 mg/ml) and mixed to prepare dispersion. The dispersion was sonicated for 6 hours using probe sonicator JY92-llN at 80 percent power (i.e. 520 W). The dispersion was centrifuged at 1500, 1000, and 500 rpm for 45 minutes. The supernatant was collected and TiB_2 nanosheets were separated from N-methyl-2-pyrrolidone through vacuum filtration. The sample was dried at 100^0C for few hours.

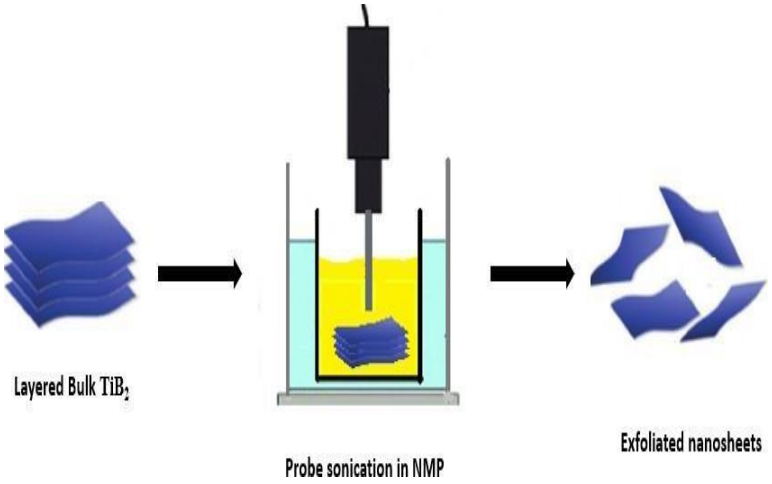

Fig. 3.3 Schematics for exfoliation of TiB_2

3.5.2 Synthesis of TiB_2@TiO_2 Nanocomposite

Commercial grade anatase TiO_2 nanoparticles (CAS 13463-67-7) were used in this synthesis process. TiO_2 NPs were mixed in of propanol and probe sonicated to make dispersion of particles. The exfoliated sheets were also sonicated in propanol. TiB_2 nanosheets were combined in 2%, 1%, and 0.5% concentration with TiO_2 nanoparticles, respectively. By combining both solutions three samples with varying concentrations of sheets were prepared. The samples were again bath sonicated for 4 hours for homogeneous mixing. Then the solution was dried at 80^0 C in oven to remove the solvent.

3.6 Characterization of Samples

The analysis of the synthesized nanosheets and nanocomposite was performed by the following characterization techniques:

3.6.1 X-Ray Diffraction (XRD)

XRD was performed using powder samples of nanosheets and nanocomposite, without involving any sample preparation step.

3.6.2 Scanning Electron Microscopy (SEM)

For SEM analysis powder samples were sonicated in ethanol for 2 hours and then drop- cast on clean glass slides followed by drying of samples at 80^0 C.

3.6.3 Atomic Force Microscopy (AFM)

AFM analysis also required sonication of powder samples in ethanol for 2 hours then drop-casting on clean silica slides and subsequent drying at 80^0 C for evaporation of ethanol.

3.6.4 UV Visible Spectroscopy

UV analysis required homogenous dispersion of powder samples. The powder samples were sonicated for 3 hours in NMP (N-Methyl-2-pyrrolidone). 2 ml of each dispersion was used for UV analysis.

The $TiB_2@TiO_2$ nanocomposites were further employed for photocatalytic degradation of Rhodamine B dye.

3.6.5 Brunauer Emmett Teller (BET)

Surface area and porosity is the vital property of a material which can be determined by BET analysis technique. For sample preparation 200 mg of sample is purified by degassing to remove the extra atmospheric contaminants like water vapors and air at 150 ^{0} C. Then the sample analysis was performed using Gemini® VII 2390 instrument. Operating conditions were degassing of the sample at $300°C$ for 3 hrs.

and analysis were performed at 0.05 to 0.3 p/p0 range.

3.7 Photocatalysis of Rhodamine B

The photocatalytic degradation efficiency of the prepared $TiB_2@TiO_2$ nanocomposites was tested by degradation of an organic dye rhodamine B. To prepare dye solution, 1 mg of Rhodamine B was taken in 1 L of deionized water and prepared a homogeneous mixture. Each $TiB_2@TiO_2$ nanocomposites sample was added in of dye solution(1mg/1ml) to study their effect on dye photodegradation. The readings of degradation are taken after 30 mins intervals.

Chapter 4

Results and discussion

TiB_2 nanosheets were successfully synthesized by liquid exfoliation of bulk TiB_2. The exfoliated nanosheets were combined with TiO_2 nanoparticles by physical mixing to make TiB_2@TiO_2 nanocomposites. The prepared TiB_2 nanosheets and TiB_2@TiO_2 nanocomposites were characterized by XRD, SEM, AFM, and UV-Visible spectroscopy. The TiB_2@TiO_2 nanocomposites were employed for testing photodegradation of rhodamine B dye. The results of these experimentation and characterizations are discussed in this section.

4.1 Characterization of TiB_2 nanosheets

To probe the structural and chemical aspects of TiB_2 bulk powder and exfoliated sheets we obtained the XRD spectra (Fig. 4.1). The bulk sample showed peaks at 27°, 34°, 44°, 57°, 61°, 68°, 71°, 78° and 88° and it was matched with JCPDS card 01-075-0967. The exfoliated samples showed peaks at 22°, 27°, 28°, 34°, 44°,57°, 64°, and 82°. The peaks at 27°, 34°, 44°, and 57° correspond to (001), (100), (101) and (002) planes and d-spacing of 3.22 Å, 2.62 Å, 2.03 Å, 1.61 Å respectively (reference card: 01-075-0967). When compared with the XRD spectrum of bulk TiB_2, it displayed two principal differences: a decrease in the intensity and broadening of peaks belonging to bulk TiB_2, and the presence of newer peaks. The reduction in intensity of peaks present in bulk TiB_2 is likely due to decrease in the number of layers, because of exfoliation. [70] The new peaks at 28°, and 64°correspond to (211), (224) planes. As a result of exfoliation, the number of layers decreases significantly resulting in the reduction of peaks original to TiB_2. [71] These exfoliated nanosheets are restacked when obtained in powder form due to which the diffraction peaks get broader, and the most intense peak corresponds to the preferred orientation. The exfoliated nanosheets cannot restack in an accurate lateral and

vertical alignment that exactly agrees with the bulk material it was derived from. Hence, the XRD results for these nanosheets, do not resemble that of the bulk material. [72]

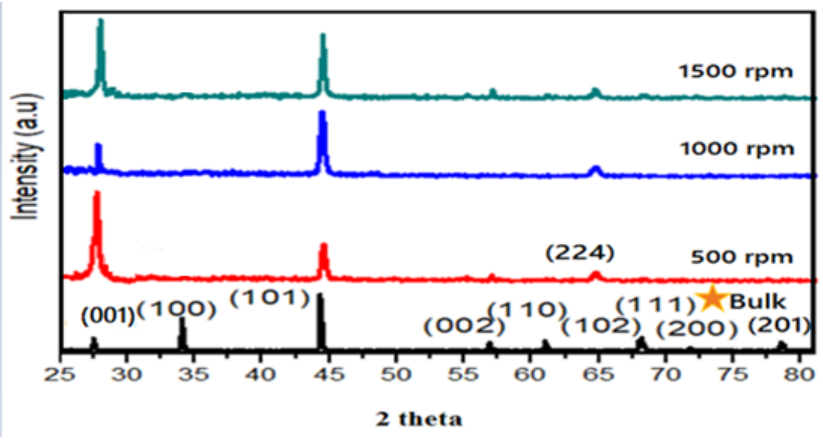

Fig. 4.1 XRD for bulk TiB_2, and exfoliated sheets at 500rpm,

1000 rpm, 1500 rpm

Atomic force microscopy was employed to further probe the morphological aspects of TiB_2 nanosheets by using JEOL-SPM 5200. The samples were prepared on clean silica slides, the nanosheets were sonicated in ethanol then drop-casting on silica slides then followed by drying for evaporation of ethanol. The AFM results (shown in Fig. 4.2, 4.3,4.4) are obtained in tapping mode. The height profiles of images show the estimated thickness of sheets at 500 rpm,1000 rpm, and 1500 rpm. The height (estimated thickness) of sheets was calculated by taking standard deviation of each sample. The estimated thickness was found to be ~15 nm thickness (Standard deviation error = 0.34) for 500 rpm, ~14 nm thickness (Standard deviation error = 0.30) for 1000 rpm, and ~12.5 nm height (Standard deviation error = 0.29) for 1500 rpm. The thickness of the flakes suggests the presence of ~ 8-12 layers molecular layers joined together via ionic and covalent bonding. [70]

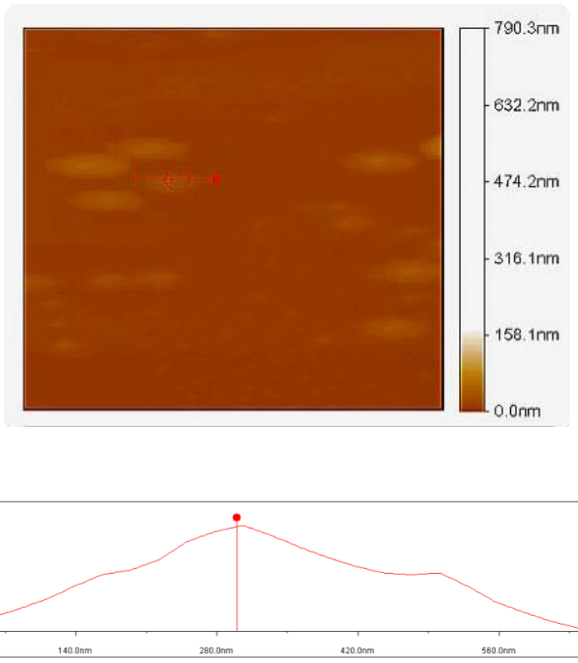

Fig. 4.2 AFM image showing thickness of exfoliated sheets at 500 rpm

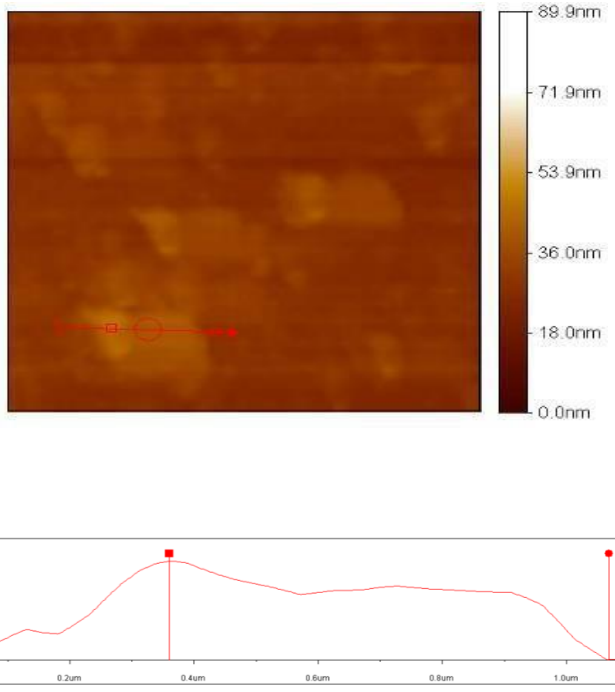

Fig. 4.3 AFM image showing thickness of exfoliated sheets at 1000 rpm

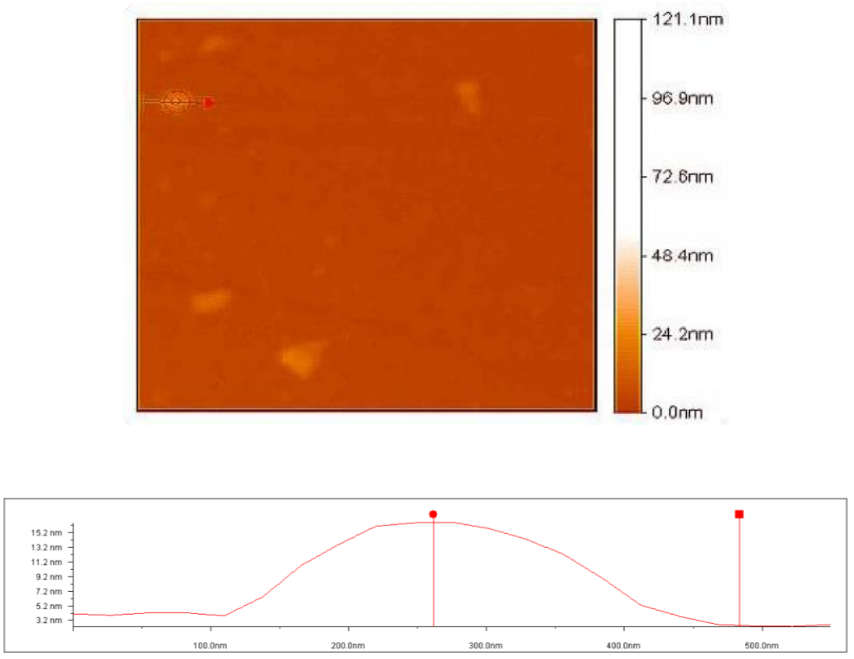

Fig. 4.4 AFM image showing thickness of exfoliated sheets at 1500 rpm

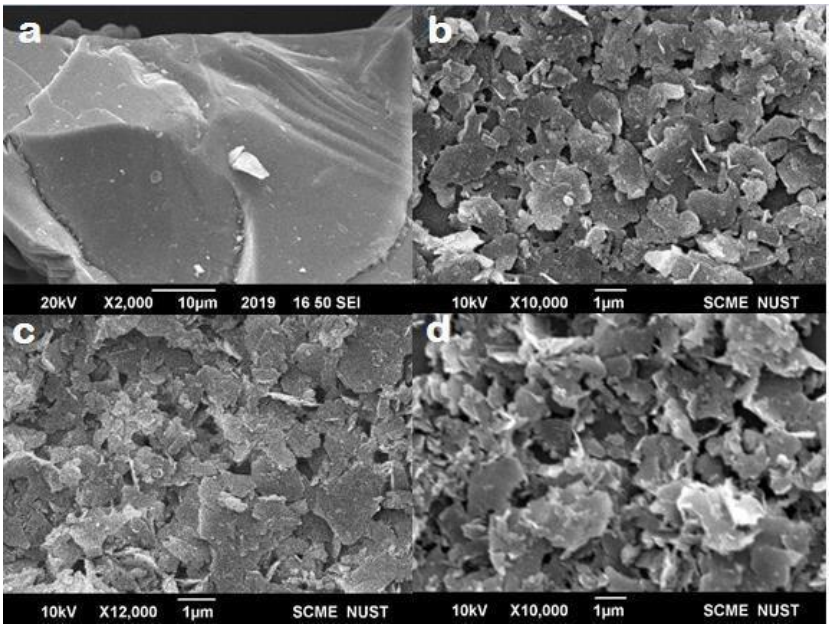

Fig. 4.5 SEM image of (a) bulk TiB_2 powder (b) exfoliated sheets at 500 rpm (c) exfoliated sheets at 1000 rpm (d) exfoliated sheets at 1500 rpm

To analyze the topography of bulk TiB_2 and exfoliated nanosheets the SEM technique was employed. Powered nanosheets were sonicated in ethanol and then drop-casted on clean glass slides and dried to completely remove ethanol. The surface topography of bulk TiB_2 powder is shown in fig. 4.5 (a), and successful exfoliated nanosheets of TiB_2 at 500 rpm (shown in fig. 4.5(b)), nanosheets at 1000 rpm (shown in fig 4.5(c)) and nanosheets at 1500 rpm (shown in fig. 4.5(d)). The average length of sheets at 500 rpm is ~ 0.81 micrometer (Standard deviation error = 0.22), at 1000 rpm is 0.77 micrometer (Standard deviation error = 0.04) and at 1500 rpm is 0.73 micrometer (Standard deviation error = 0.03). So, it can be concluded that the nanosheets prepared by liquid phase exfoliation method possess with lateral dimensions of high aspect ratio sheets are of the order of few microns.

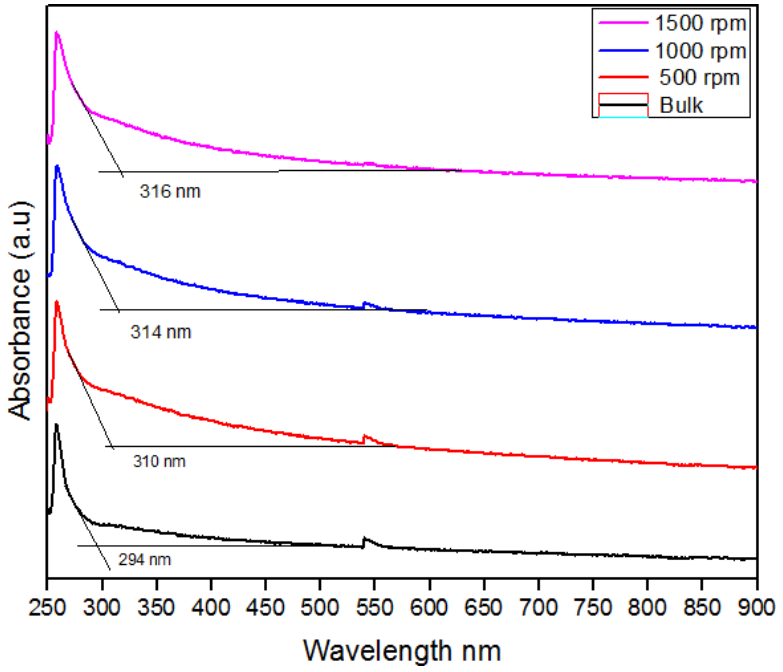

Fig.4.6 Absorption onset values for bandgap estimation of the bulk TiB_2 powder, and exfoliated nanosheets at 500rpm, 1000 rpm and 1500 rpm

The optical absorption spectrum of bulk and exfoliated samples was obtained using Jenway 7315 (Fig.4.6). A dispersion of bulk and exfoliated powder samples was prepared in NMP (N-methyl- 2-pyrrolidone). The bulk TiB_2 shows a sharp absorption edge in the UV region at 256 nm.

The peaks for exfoliated samples show peak broadening resulting into red shift and offering more absorption in this region. The exfoliated sheets at 500 rpm, 1000 rpm, and 1500 rpm show absorption peaks at ~ 258 nm. [24]

The absorption onset values are situated in the UV region, at 274 nm, 276 nm, 280 nm ,281 nm for bulk TiB_2, nanosheets at 500 rpm, 1000 rpm and 1500 rpm respectively. The UV-Vis spectrum of the samples manifests a possibility of employing these nanosheets as UV absorbing photoactive material. Through the transition of the bulb from UV light to visible light in the spectrophotometer, a small peak at 550 nm emerged, it is considered as a device error.

The bandgap estimation of the bulk and exfoliated sheets, direct bandgap extrapolation technique was used to draw tauc plots for band gap estimation of bulk titanium diboride and the exfoliated nanosheets. The estimated direct bandgap for the bulk Titanium diboride is 3.7 eV and for exfoliated samples, it's 3.9 eV.

4.2 Characterization of TiB_2@TiO_2 nanocomposite

The TiB_2@TiO_2 nanocomposite was analyzed by XRD as shown in Fig.4.7. XRD analysis shows peaks to TiO_2 at 25 º,27 º,38 º,47 º,53 º,54 º,62 º, 68 º,70 º, and 74º. Majority of the peaks show anatase phase of titania, however peaks at 27 º,53 º and 62º show rutile phase. As majority of the peaks belong to anatase phase, these TiO_2 nanoparticles will show good photocatalytic response. The peaks at 44^0, and 82^0 in the composite sample belong to Titanium diboride and were matched with JCPDS card 01-089-3923.

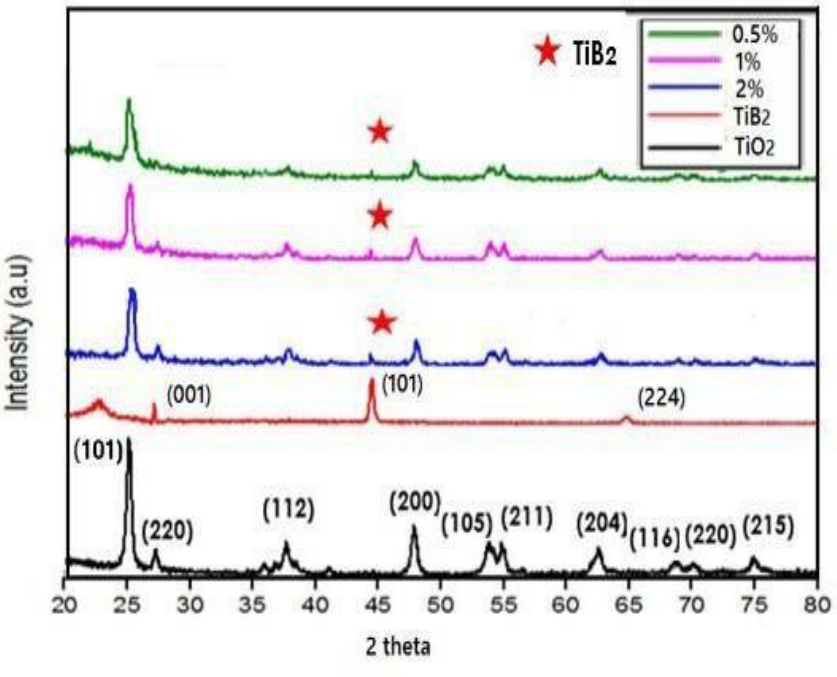

Fig.4.7 XRD for TiO2 Nps, TiB_2 sheets and TiB_2@TiO_2 nanocomposite with 2%, 1%, and 0.5 % TiB_2 nanosheets

These peaks have very low intensity as the amount of TiB_2 (0.5%, 1% and 2%) in these samples was considerably less as compared to TiO_2. The remaining peaks in the sample belong to TiO_2, and they were matched with JCPDS card 01-071-1168. The intensity of these peaks was also reduced as compared to pure TiO_2 peaks. All the peaks in the sample belong to TiB_2 and TiO_2 thus, leading to successful synthesis of the composite material without any impurity.

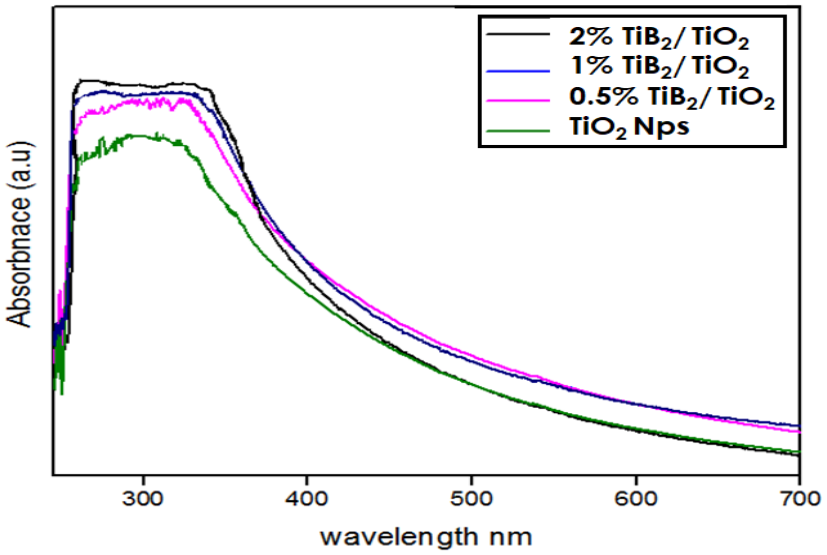

Fig.4.8 UV Visible Spectrum of TiO_2 nanoparticles and TiB_2@ TiO_2 nanocomposites

UV-Vis Spectroscopy was performed to analyze the photo-response of the material when exposed to light. TiB_2 nanosheets composites showed strong absorption in UV region of solar spectrum which means the samples will show strong photocatalytic activity in UV light irradiation shown in Fig.4.8. The UV visible spectrum of the prepared TiB_2@ TiO_2 nanocomposites (0.5%,1%,2% TiB_2 sheets) showed increase in the UV absorption region, as compared to the titania nanoparticles. This shows that by increasing the amount of TiB_2 nanosheets, the absorption region increases. TiB_2 is a good conductor, it can assist in reducing the charge recombination rate and TiB_2 nanosheets with provide additional reaction sites for the dye molecules. Thus, TiB_2 has a vital role in enhancing the photocatalytic activity in these composites. TiO_2 can be used as a sensitizer as i.e., electrons from CB of TiO_2 generated due to UV light absorption can be easily transferred to the TiB_2. As TiB_2 offers good conductivity thus, it becomes capable of UV light photocatalysis. So, the prepared nanocomposites ought to show better photocatalytic properties under UV light as compared to titania NPs.

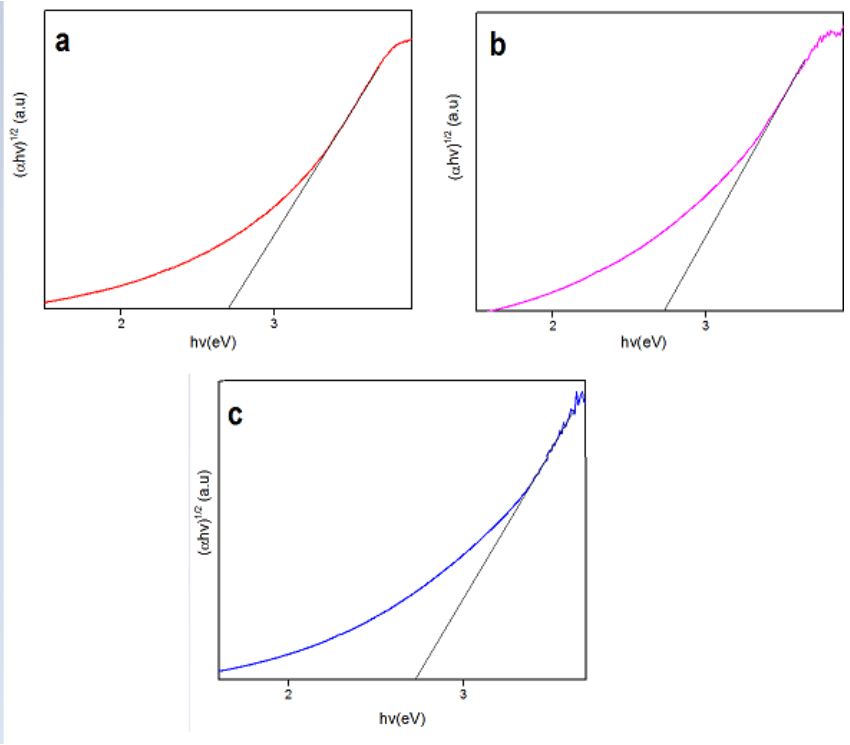

Fig.4.9 Tauc plot of the TiB_2/ TiO_2 nanocomposite with (a) 2%, (b) 1%, and (c) 0.5 % TiB_2 nanosheets

The UV visible spectroscopy was performed for the prepared nanocomposites shown in Fig.4.9. For bandgap calculation, tauc plot method was employed. The estimated indirect bandgap of these nanocomposites was found to be 2.7 eV. Which shows bandgap tunning of the titania NPs, the bandgap of anatase titania NPs was 3.3 eV. As titania could absorb only the ultraviolet region of the electromagnetic spectrum due to its large band gap, tunning of band gap enables the composite to utilize more solar energy.

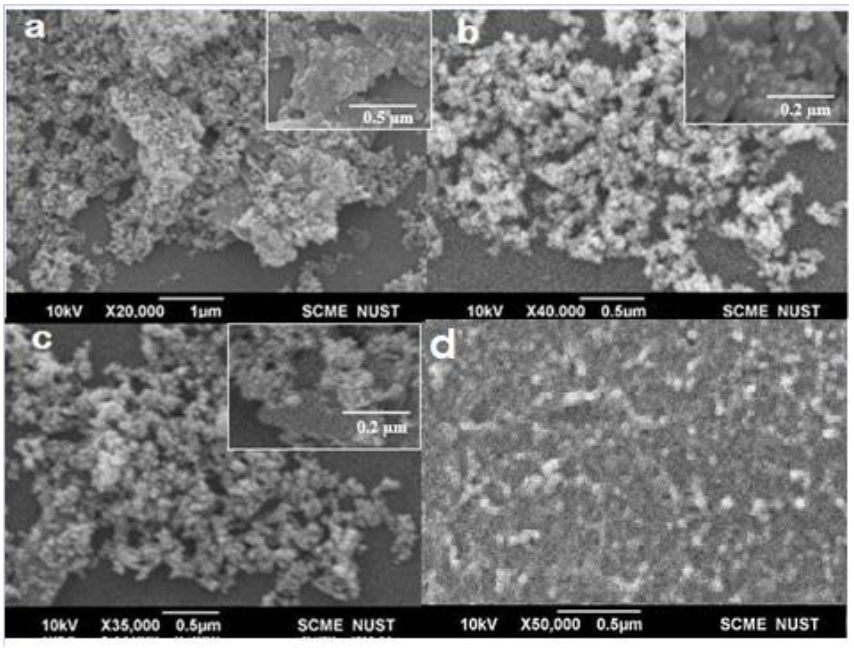

Fig. 4.10 SEM image of TiB_2@TiO_2 nanocomposite(a) 2% (b) 1% (c) 0.5% nanosheets (d) TiO_2 Nps

The structural and morphological analysis of the prepared nanocomposite was performed by SEM as shown in Fig. 4.10. The results show presence of both sheets and nanoparticles in the sample. The size of nanoparticles is 30 nm to 45 nm shown in fig. 4.10 (d). The inset images show closeup of the samples, the nanosheets were loaded with nanoparticles as shown in fig. 4.10 (a), (b), (c). The presence of nanosheets became more visible with subsequent increase of 0.5%, 1%, and 2% nanosheets. The SEM results show successful synthesis of nanocomposite with homogeneous distribution of nanoparticles.

The BET analysis was performed to analyze specific surface area of the samples. The composite samples showed increase in their surface area with the addition of nanosheets in titania powder. The surface area of TiO_2 Nanoparticles was 36.66(m^2/g) which gradually improved with the addition of nanosheets. The increase in surface area of composites with be helpful in photocatalysis as it provides more reaction sites.

Table 5: BET of TiO_2 and TiO_2/ TiB_2 nanocomposites to determine surface area

Samples	**Surface area (m^2/g)**
TiO_2 Nanoparticles	36.66
TiO_2/TiB_2 0.5%	41.16
TiO_2/ TiB_2 1%	50.69
TiO_2/ TiB_2 2%	53.35

4.3 Photocatalysis of Rhodamine B

Photodegradation activity of organic dye, i.e., Rhodamine B (RhB) was observed in a UV photocatalytic reactor at room temperature. UV-A lights of 15 W having wavelength range starting from 320 nm to a visible light cut-off at 380 nm were employed. The dye solution was prepared by mixing 1 mg of Rhodamine B in 1 L of deionized water. TiO_2 nanoparticles and TiB_2@TiO_2 nanocomposites samples were added in 50 ml of dye solution to study their effect on dye photodegradation.

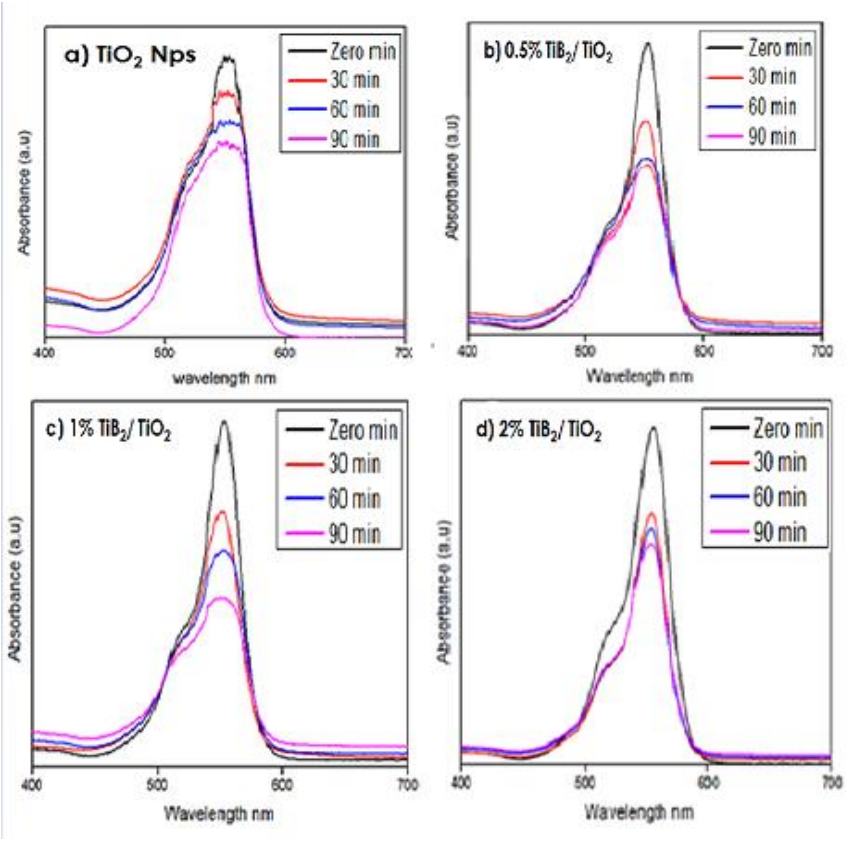

Fig. 4.11 UV–Vis spectra of photodegradation of RhB by (a) TiO_2 nanoparticles and TiB_2@TiO_2 nanocomposites (b) 0.5 % TiB_2 nanosheets (c) 1% TiB_2 nanosheets (d) 2 % TiB_2 nanosheets

The UV -Vis graph showing photocatalytic degradation of RhB aqueous solution using the TiO_2 nanoparticles and prepared TiB_2@TiO_2 nanocomposites in terms of declining intensity of absorption as shown in Fig. 4.11. The notable variations in RhB concentrations were investigated by estimating the intensity differences of the maximal absorption peak λ max at 554 nm and applying Beer-Lambert law in the obtained UV visible spectrum. The strength of the absorption peak at 554 nm appeared to be decreasing and showing a slight blue shift, with prolonging exposure time for irradiation, thus establishing the degradation efficiency. TiO_2 nanoparticles showed 34% degradation of rhodamine B in 90 minutes as shown in fig. 4.11 (a). The sample with 1% of TiB_2 nanosheets showed maximum degradation of RhB, as the percentage of TiB_2 nanosheets increased from 1% to 2% the efficiency of

photocatalytic degradation of RhB decreased. With 2% TiB_2 nanosheets nanocomposite, the sample showed least photocatalytic activity due to accumulation of sheets and non-photocatalytic behavior of TiB_2. The results show favorable photocatalytic efficiency which means that recombination rate of photo-induced charge carriers has decreased thus extended its lifetime. [29]

These photoinduced degradation reactions usually follow first order reaction kinetics which is given by:

$\ln C/C_0 = kKt = kt,$

here, k is the first-order rate constant. [73]

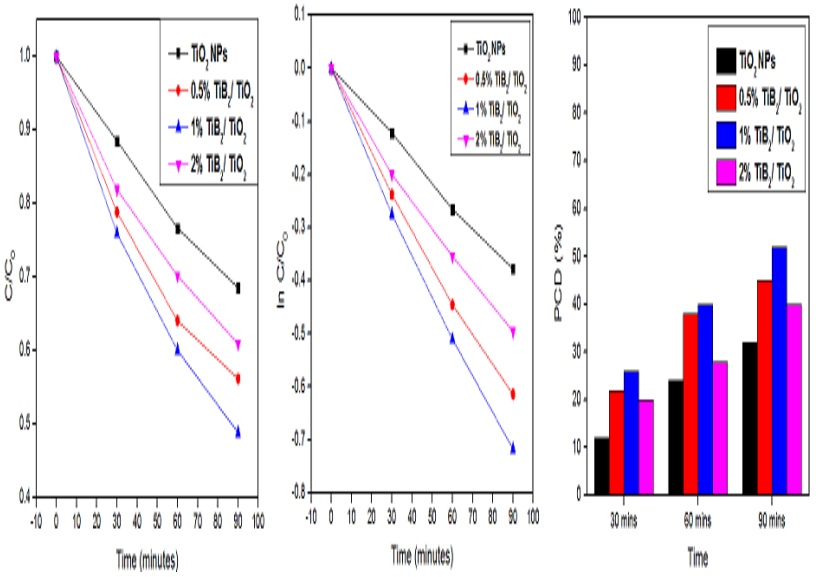

Fig. 4.12 Photodegradation of Rhodamine B (a) as a function of C/C_0 (b) Log plots of degradation efficiency to determine the rate constant (c) Percentage degradation of Rhodamine B as a function of increasing time

Figure 4.12 (a) shows photodegradation of Rhodamine B as a function of C_t/C_0 and fig. 4.12 (b) shows Log plots of degradation efficiency the rate constant determination. The photocatalytic degradation efficiency (PCD) was calculated using

the Eq.1.

$$\% \text{ Degradation} = (1 - C_t/C_0) \times 100 \quad (1)$$

The maximum efficiency of 52 % was achieved by the sample with 1% of TiB_2 nanosheets. The catalyst with 0.5% and 2% of TiB_2 nanosheets have shown 45% and 39 % maximum degradation efficiency in 90 minutes as shown in Fig. 4.12 (c).

Based on above analysis, the plausible photo-response mechanism is proposed. As TiO_2 is sensitive to UV light, under illumination electron-hole pairs were generated. Under UV light, electron in the valance band get transfer to conduction band in the photocatalyst as corresponding energy is higher than the band gap of TiO_2 (bandgap value) which promotes the generation of electrons (e-) in conduction band and holes (h+) in valance bond.

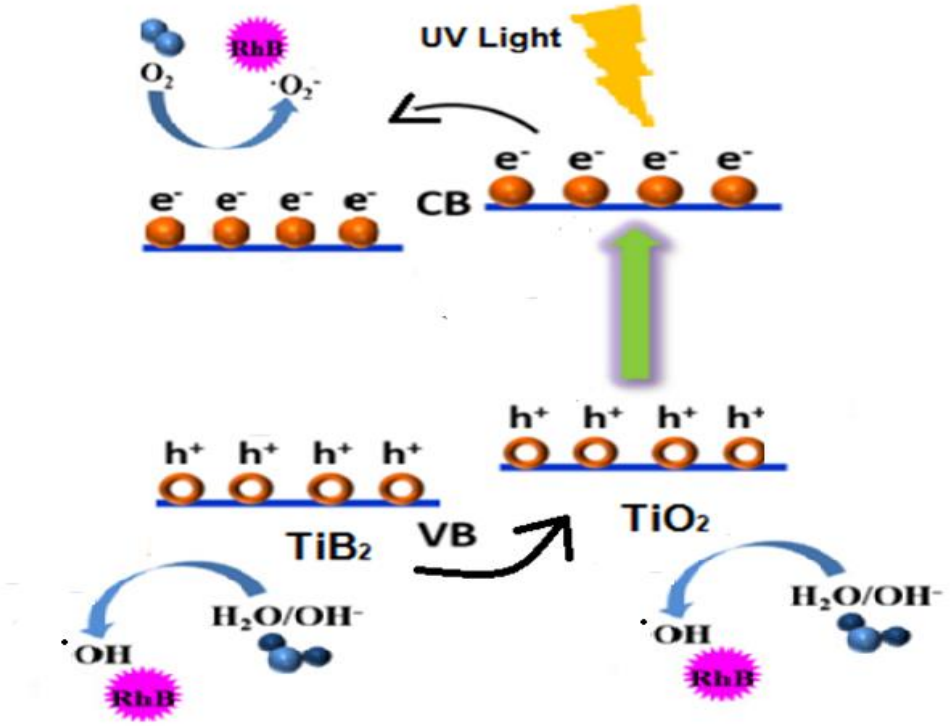

Figure.4.13 Schematics of TiO_2@TiB_2 photodegradation

The photogenerated holes can directly oxidize the dye or they can react with H_2O molecules or OH- ions to form hydroxyl radicals (·OH). Also, the photoelectrons on the catalyst surface reduces oxygen molecules to superoxide radicals ($\bullet O_2$-). So finally, the dye molecules were degraded by the generation of ·OH and $\bullet O_2$-. The mechanism is given as follows:

$TiO_2 + h\nu \rightarrow h^+ + e^-$

$h^+ + OH^-/H_2O \rightarrow \cdot OH$

$e^- + \bullet O_2^- \rightarrow \bullet O_2^-$

$\bullet OH$ and $\bullet O_2^-$ + dye molecules $\rightarrow CO_2 + H_2O$ + inorganic acids.

Conclusion

Titanium diboride nanosheets were successfully synthesized by liquid phase exfoliation. The synthesized sheets with high aspect ratio of few microns were characterized by XRD, UV-Vis spectroscopy, AFM, and SEM. The characterization techniques verified the exfoliation of bulk titanium diboride into 2D nanosheets. XRD analysis showed presence of new peaks in exfoliated samples confirming formation of 2D sheets. The absorption onset values situated in the UV region, from 276 nm to 281 nm for nanosheets, suggested employing these nanosheets as UV absorbing photoactive material. AFM and SEM results showed thickness of sheets less than 15nm and length approximately 0.8 micrometers. The UV- visible graph showed maximum absorbance in UV region of the spectrum. For photocatalytic degradation testing, titanium diboride nanosheets were combined with titania nanoparticles to prepare a photocatalyst material. Commercial titania nanoparticles were used to make $TiB_2@TiO_2$ nanocomposite. The composite was tested for photocatalytic degradation of Rhodamine B dye. We have successfully produced $TiB_2@TiO_2$ nanocomposite, with ex situ technique. The composite catalyst successfully degraded 51% of RhB in 90 minutes. However, to further enhance its efficiency it can be made via in situ route. TiB_2 nanosheets can be functionalized or combined with materials (i.e., TiC) and make structural modifications (e.g., porous structure) to make it visible light active photocatalyst.

Future Recommendation

In this project, the TiB_2 nanosheets were synthesized and employed for making $TiB_2@TiO_2$ nanocomposite for photocatalytic application. However, in future, TiB_2 nanosheets can be functionalized or combined with materials (i.e., TiC) and make structural modifications (e.g., porous structure) to make it visible light active photocatalyst.

Titanium diboride possesses properties like hardness, chemical inertness, oxidation resistance and high conductivity both thermally and electrically. The TiB_2 nanosheets we can extend these advantages to nanoscale devices and products, for instance, electrodes, aircraft materials, durable electronics, and heterostructures incorporating other nanomaterials.

References

[1] K. Shingange, Z. P. Tshabalala, B. P. Dhonge, O. M. Ntwaeaborwa, D. E. Motaung, and G.H. Mhlongo, "0D to 3D ZnO nanostructures and their luminescence, magnetic and sensing properties: Influence of pH and annealing," *Mater. Res. Bull.*, vol. 85, pp. 52–63, (2017), doi: 10.1016/j.materresbull.(2016).09.003.

[2] S. Liu *et al.*, "Enhanced Photocatalytic Degradation of Environmental Pollutants under Visible Irradiation by a Composite Coating," *Environ. Sci. Technol.*, vol. 51, no. 9, pp. 5137–5145, (2017), doi: 10.1021/acs.est.7b00350.

[3] P. Mazierski, A. Mikolajczyk, B. Bajorowicz, A. Malankowska, A. Zaleska-Medynska, and J. Nadolna, "The role of lanthanides in TiO2-based photocatalysis: A review," *Appl. Catal. B Environ.*, vol. 233, pp. 301–317, (2018), doi: 10.1016/j.apcatb. (2018).04.019.

[4] G. Nabiyouni, M. J. Fesharaki, M. Mozafari, and J. Amighian, "Characterization and magnetic properties of nickel ferrite nanoparticles prepared by ball milling technique," *Chinese Phys. Lett.*, vol. 27, no. 12, pp. 10–14, (2010), doi: 10.1088/0256- 307X/27/12/126401.

[5] R. Valenzuela, "Novel applications of ferrites," *Phys. Res. Int.*, vol. (2012), (2012), doi: 10.1155/2012/591839.

[6] R. Mas-Ballesté, C. Gómez-Navarro, J. Gómez-Herrero, and F. Zamora, "2D materials: To graphene and beyond," *Nanoscale*, vol. 3, no. 1, pp. 20–30, (2011), doi: 10.1039/c0nr00323a.

[7] Z. Wang, T. Hu, R. Liang, and M. Wei, "Application of Zero-Dimensional Nanomaterials in Biosensing," *Front. Chem.*, vol. 8, no. April, pp. 1–19, (2020), doi: 10.3389/fchem. (2020).00320.

[8] R. Rajendran, L. K. Shrestha, K. Minami, M. Subramanian, R. Jayavel, and K. Ariga, "Dimensionally integrated nanoarchitectonics for a novel composite from 0D, 1D, and 2D nanomaterials: RGO/CNT/CeO2 ternary nanocomposites with electrochemical performance," *J. Mater. Chem. A*, vol. 2, no. 43, pp. 18480–18487, (2014), doi: 10.1039/c4ta03996c.

[9] D. Ziental *et al.*, "Titanium dioxide nanoparticles: Prospects and applications in

medicine," *Nanomaterials*, vol. 10, no. 2, (2020), doi: 10.3390/nano10020387.

[10] C. H. Tsai, C. M. Lin, and Y. C. Liu, "Increasing the effciency of dye-sensitized solar cells by adding nickel oxide nanoparticles to titanium dioxideworking electrodes," *Coatings*, vol. 10, no. 2, pp. 1–13, (2020), doi: 10.3390/coatings10020195.

[11] X. Dong, H. Youssef, Y. Zhang, H. Yang, S. Wang, and S. Ji, "Advanced heat treated die- cast aluminium composites fabricated by TiB2 nanoparticle implantation," *Mater. Des.*, vol. 186, p. 108372, (2020), doi: 10.1016/j.matdes. (2019).108372.

[12] N. Abu-Warda, M. D. López, M. D. Escalera-Rodríguez, E. Otero, and M. V. Utrilla, "Corrosion behavior of mechanically alloyed A6005 aluminum alloy composite reinforced with TiB2 nanoparticles," *Mater. Corros.*, vol. 71, no. 3, pp. 382–391, (2020), doi: 10.1002/maco. (2019)11174.

[13] Y. Gu, Y. Qian, L. Chen, and F. Zhou, "A mild solvothermal route to nanocrystalline titanium diboride," *J. Alloys Compd.*, vol. 352, no. 1–2, pp. 325–327, (2003), doi: 10.1016/S0925-8388(02)01173-8.

[14] A. Javadi, S. Pan, C. Cao, G. Yao, and X. Li, "Facile synthesis of 10 nm surface clean TiB2 nanoparticles," *Mater. Lett.*, vol. 229, no. June, pp. 107–110, (2018), doi: 10.1016/j.matlet. (2018).06.054.

[15] A. Rabiezadeh, A. M. Hadian, and A. Ataie, "Preparation of alumina/titanium diboride nano-composite powder by milling assisted sol-gel method," *Int. J. Refract. Met. Hard Mater.*, vol. 31, pp. 121–124, (2012), doi: 10.1016/j.ijrmhm. (2011).09.015.

[16] D. H. Chen and X. R. He, "Synthesis of nickel ferrite nanoparticles by sol-gel method," *Mater. Res. Bull.*, vol. 36, no. 7–8, pp. 1369–1377, (2001), doi: 10.1016/S0025- 5408(01)00620-1.

[17] Y. Liu, X. Liu, and Z. Zhang, "Preparation and microwave absorption property of nickel spinel ferrite," *Key Eng. Mater.*, vol. 531–532, pp. 36–39, 2013, doi: 10.4028/www.scientific.net/KEM.531-532.36.

[18] M. Dang, M. Liu, and F. Li, "Mesoporous 3D titanium dioxide embed carbon nanofibers with superior polysulfide adsorption ability for high electrochemical

performance Li-S batteries," *Ionics (Kiel).*, vol. 27, no. 4, pp. 1531–1536, (2021), doi: 10.1007/s11581-021- 03937-x.

[19] F. Huang, A. Yan, Z. Fu, S. Yin, F. Zhang, and Y. Qiang, "Self-assembled synthesis of TiO2/TiB2 nanowall and its photocatalytic properties," *J. Alloys Compd.*, vol. 574, pp. 49– 53, (2013), doi: 10.1016/j.jallcom. (2013).04.063.

[20] F. Huang *et al.*, "Several shape-controlled TiO2/TiB2 hybrid materials with a combined growth mechanism," *Mater. Lett.*, vol. 63, no. 30, pp. 2655–2658, (2009), doi: 10.1016/j.matlet. (2009).09.027.

[21] H. Zhang, H. M. Cheng, and P. Ye, "2D nanomaterials: Beyond graphene and transition metal dichalcogenides," *Chem. Soc. Rev.*, vol. 47, no. 16, pp. 6009–6012, (2018), doi: 10.1039/c8cs90084a.

[22] P. Ganguly *et al.*, "2D Nanomaterials for Photocatalytic Hydrogen Production," *ACS Energy Lett.*, vol. 4, no. 7, pp. 1687–1709, (2019), doi: 10.1021/acsenergylett.9b00940.

[23] S. K. John and A. A. Anappara, "Aqueous dispersions of highly luminescent boron-rich nanosheets by the exfoliation of polycrystalline titanium diboride," *New J. Chem.*, vol. 43, no. 25, pp. 9953–9960, (2019), doi: 10.1039/c9nj01502g.

[24] K. H. Wu, Y. Wang, Yu-Jiang, G. H. Zhang, S. Q. Jiao, and K. C. Chou, "Low temperature synthesis of titanium diboride nanosheets by molten salt–assisted borothermal reduction of TiO2," *J. Nanoparticle Res.*, vol. 21, no. 5, (2019), doi: 10.1007/s11051-019-4560-z.

[25] H. Y. Zhai, H. M. Christen, C. Cantoni, A. Goyal, and D. H. Lowndes, "Epitaxial titanium diboride films grown by pulsed-laser deposition," *Appl. Phys. Lett.*, vol. 80, no. 11, pp. 1963–1965, (2002), doi: 10.1063/1.1461869.

[26] J. Šubrt *et al.*, "Highly photoactive 2D titanium dioxide nanostructures prepared from lyophilized aqueous colloids of peroxo-polytitanic acid," *Mater. Res.Bull.*,vol.49,no.1,pp.405–412,(2014),doi:10.1016/j.materresbull (2013).09.028.

[27] F. Long *et al.*, "Synergistic strengthening effect of carbon nanotubes (CNTs) and titanium diboride (TiB2) microparticles on mechanical properties of copper

matrix composites," *J. Mater. Res. Technol.*, vol. 9, no. 4, pp. 7989–8000, (2020), doi: 10.1016/j.jmrt. (2020).05.036.

[28] T. Cong *et al.*, "Extremely sensitive and reusable surface-enhanced Raman scattering substrate based on 3D Ag-titanium dioxide nanowires," *J. Alloys Compd.*, vol. 859, p. 158389, (2021), doi: 10.1016/j.jallcom. (2020).158389.

[29] D. M. Tobaldi, R. C. Pullar, A. S. Škapin, M. P. Seabra, and J. A. Labrincha, "Visible light activated photocatalytic behaviour of rare earth modified commercial TiO2," *Mater. Res. Bull.*, vol. 50, pp. 183–190, (2014), doi: 10.1016/j.materresbull. (2013).10.033.

[30] W. Wang, M. O. Tadé, and Z. Shao, "Nitrogen-doped simple and complex oxides for photocatalysis: A review," *Prog. Mater. Sci.*, vol. 92, pp. 33–63, (2018), doi: 10.1016/j.pmatsci. (2017).09.002.

[31] K. Singh *et al.*, "Erbium doped TiO 2 interconnected mesoporous spheres as an efficient visible light catalyst for photocatalytic applications," *Appl. Surf. Sci.*, vol. 449, pp. 755– 763, (2018), doi: 10.1016/j.apsusc. (2018).01.279.

[32] A. Baruah, V. Chaudhary, R. Malik, and V. K. Tomer, *17 -Nanotechnology Based Solutions for Wastewater Treatment*. Elsevier Inc., (2018).

[33] S. Weon and W. Choi, "TiO2 Nanotubes with Open Channels as Deactivation-Resistant Photocatalyst for the Degradation of Volatile Organic Compounds," *Environ. Sci. Technol.*, vol. 50, no. 5, pp. 2556–2563, (2016), doi: 10.1021/acs.est.5b05418.

[34] F. Petronella, A. Truppi, M. Dell'Edera, A. Agostiano, M. L. Curri, and R. Comparelli, "Scalable synthesis of mesoporous TiO2 for environmental photocatalytic applications," *Materials (Basel).*, vol. 12, no. 11, (2019), doi: 10.3390/ma12111853.

[35] J. K. Kim, J. J. Kim, and J. C. Joo, " Preparation of Nano Spinel Doped TiO2 and Its Photocatalytic Activity Evaluation Under Visible Light Irradiation ," *J. Nanosci. Nanotechnol.*, vol. 19, no. 2, pp. 1137–1140, (2018), doi: 10.1166/jnn. (2019).15962.

[36] L. Zheng, W. Zhang, and X. Xiao, "Preparation of titanium dioxide/tungsten disulfide composite photocatalysts with enhanced photocatalytic activity under

visible light," *Korean J. Chem. Eng.*, vol. 33, no. 1, pp. 107–113, (2016), doi: 10.1007/s11814-015-0098-7.

[37] D. M. De Los Santos *et al.*, "Study of thulium doping effect and enhancement of photocatalytic activity of rutile TiO2 nanoparticles," *Mater. Chem. Phys.*, vol. 161, pp. 175–184, (2015), doi: 10.1016/j.matchemphys. (2015).05.034.

[38] C. H. A. Tsang *et al.*, "Titanium oxide based photocatalytic materials development and their role of in the air pollutants degradation: Overview and forecast," *Environ. Int.*, vol. 125, no. January, pp. 200–228, (2019), doi: 10.1016/j.envint. (2019).01.015.

[39] M. Estruga, L. Chen, H. Choi, X. Li, and S. Jin, "Ultrasonic-assisted synthesis of surface- clean TiB2 nanoparticles and their improved dispersion and capture in al-matrix nanocomposites," *ACS Appl. Mater. Interfaces*, vol. 5, no. 17, pp. 8813–8819, (2013), doi: 10.1021/am402719p.

[40] E. Sani *et al.*, "Titanium diboride ceramics for solar thermal absorbers," *Sol. Energy Mater. Sol. Cells*, vol. 169, pp. 313–319, (2017), doi: 10.1016/j.solmat.2017.05.038.

[41] L. Silvestroni, H. J. Kleebe, W. G. Fahrenholtz, and J. Watts, "Super-strong materials for temperatures exceeding 2000 °c," *Sci. Rep.*, vol. 7, no. December (2016), pp. 1–8, (2017), doi: 10.1038/srep40730.

[42] M. M. Opeka, I. G. Talmy, and J. A. Zaykoski, "Oxidation-based materials selection for 2000°C + hypersonic aerosurfaces: Theoretical considerations and historical experience," *J. Mater. Sci.*, vol. 39, no. 19, pp. 5887–5904, (2004), doi: 10.1023/B:JMSC.0000041686.21788.77.

[43] C. M. T. Sanchez, B. R. Plata, M. E. H. M. da Costa, and F. L. Freire, "Titanium diboride thin films produced by dc-magnetron sputtering: Structural and mechanical properties," *Surf. Coatings Technol.*, vol. 205, no. 12, pp. 3698–3702, (2011), doi: 10.1016/j.surfcoat. (2011).01.014.

[44] H. J. Juretschke and R. Steinitz, "Hall effect and electrical conductivity of transition-metal diborides," *J. Phys. Chem. Solids*, vol. 4, no. 1–2, pp. 118–127, (1958), doi: 10.1016/0022- 3697(58)90201-4.

[45] P. Vajeeston, P. Ravindran, C. Ravi, and R. Asokamani, “Electronic structure, bonding, and ground-state properties of AlB2-type transition-metal diborides,” *Phys. Rev. B - Condens. Matter Mater. Phys.*, vol. 63, no. 4, pp. 1–12, (2001), doi: 10.1103/PhysRevB.63.045115.

[46] M. Schneider *et al.*, “Heat and charge transport properties of MgB2,” *Phys. C Supercond. its Appl.*, vol. 363, no. 1, pp. 6–12, (2001), doi: 10.1016/S0921-4534(01)00947-9.

[47] B. Cristina and Y. Tsutomu, “Review of the superconducting properties of MgB2,” *Supercond. Sci. Technol.*, vol. 14, no. 11, p. R115, (2001), [Online]. Available: http://stacks.iop.org/0953-2048/14/i=11/a=201.

[48] I. R. Shein and A. L. Ivanovskii, “Elastic properties of mono-and polycrystalline hexagonal AlB 2-like diborides of s, p and d metals from first-principles calculations,” *J. Phys. Condens. Matter*, vol. 20, no. 41, (2008), doi: 10.1088/0953-8984/20/41/415218.

[49] J. W. Lawson, C. W. Bauschlicher, and M. S. Daw, “Ab initio computations of electronic, mechanical, and thermal properties of ZrB2 and HfB2,” *J. Am. Ceram. Soc.*, vol. 94, no. 10, pp. 3494–3499, (2011), doi: 10.1111/j.1551-2916.2011.04649.x.

[50] E. Spear, “BONDING The chemical bonding in AlBa-type metal diboride phases is considered from a crystal chemical viewpoint. The ability of metals to deform from a spherical shape appears to be very important in explaining why the diboride is formed by such a wide v,” vol. 47, pp. 195–201, (1976).

[51] L. Sun, Y. Gao, B. Xiao, Y. Li, and G. Wang, “Anisotropic elastic and thermal properties of titanium borides by first-principles calculations,” *J. Alloys Compd.*, vol. 579, pp. 457– 467, (2013), doi: 10.1016/j.jallcom. (2013).06.119.

[52] A. Waśkowska *et al.*, “Thermoelastic properties of ScB2, TiB2, YB 4 and HoB4: Experimental and theoretical studies,” *Acta Mater.*, vol. 59, no. 12, pp. 4886–4894, (2011), doi: 10.1016/j.actamat. (2011).04.030.

[53] H. Y. Yan, Q. Wei, S. M. Chang, and P. Guo, “A first-principle calculation of structural, mechanical and electronic properties of titanium borides,” *Trans. Nonferrous Met. Soc. China (English Ed.*, vol. 21, no. 7, pp. 1627–1633,

(2011), doi: 10.1016/S1003- 6326(11)60906-0.

[54] R. G. Munro, “Material Properties of Titanium Diboride,” *J. Res. Natl. Inst. Stand. Technol.*, vol. 105, no. 5, pp. 709–720, 2000, doi: 10.6028/jres.105.057.

[55] A. Yousaf *et al.*, “Exfoliation of Two-Dimensional Nanosheets of Metal Diborides,” pp. 1– 32, (2020), [Online]. Available: http://arxiv.org/abs/(2001).09237.

[56] M. Karbalaei Akbari, K. Shirvanimoghaddam, Z. Hai, S. Zhuiykov, and H. Khayyam, “Nano TiB2 and TiO2 reinforced composites: A comparative investigation on strengthening mechanisms and predicting mechanical properties via neural network modeling,” *Ceram. Int.*, vol. 43, no. 18, pp. 16799–16810, (2017), doi: 10.1016/j.ceramint. (2017).09.077.

[57] M. Khajehzadeh *et al.*, “Fabrication and Characterization of In Situ Zn-TiB2 Nanocomposite,” *Ceram. Int.*, vol. 71, no. 10, pp. 23–35, (2020), doi: 10.1063/1.5129817.

[58] X. Huang *et al.*, “In-situ formation of ultrafine MgNi3B2 and TiB2 nanoparticles: Heterogeneous nucleating and grain coarsening retardant agents for magnesium borate in Li–Mg–B–H reactive hydride composite,” *Int. J. Hydrogen Energy*, vol. 44, no. 50, pp. 27529–27541, (2019), doi: 10.1016/j.ijhydene. (2019).08.222.

[59] F. Sajedi Alvar, M. Heydari, A. Kazemzadeh, M. R. Vaezi, and L. Nikzad, “Synthesis and characterization of corrosion-resistant and biocompatible Al2O3–TiB2 nanocomposite films on pure titanium,” *Ceram. Int.*, vol. 46, no. 4, pp. 4215–4221, (2020), doi: 10.1016/j.ceramint. (2019).10.140.

[60] R. Y. He, J. Jiang, R. F. Wang, Y. Yue, Y. Chen, and T. J. Pan, “Anti-corrosion and conductivity of titanium diboride coating on metallic bipolar plates,” *Corros. Sci.*, vol. 170, no. March, (2020), doi: 10.1016/j.corsci.(2020).108646.

[61] J. Lin, Y. Yang, H. Zhang, F. Li, G. Huang, and J. Wang, “Effect of catalyst on carbon nanotubes synthesis on titanium diboride via chemical vapor deposition,” *J. Am. Ceram. Soc.*, vol. 103, no. 8, pp. 4691–4699, (2020), doi: 10.1111/jace.17128.

[62] C. S. Lim, Z. Sofer, V. Mazánek, and M. Pumera, “Layered titanium diboride: towards exfoliation and electrochemical applications,” *Nanoscale*, vol. 7, no. 29, pp. 12527–12534, (2015), doi: 10.1039/c5nr02692j.

[63] A. Rabiezadeh, A. M. Hadian, and A. Ataie, “Synthesis and sintering of TiB2 nanoparticles,” *Ceram. Int.*, vol. 40, no. 10, pp. 15775–15782, (2014), doi: 10.1016/j.ceramint.(2014).07.102.

[64] Ľ. Bača and N. Stelzer, “Adapting of sol-gel process for preparation of TiB2 powder from low-cost precursors,” *J. Eur. Ceram. Soc.*, vol. 28, no. 5, pp. 907–911, (2008), doi: 10.1016/j.jeurceramsoc.(2007).09.028.

[65] E. Kubiňáková, M. Benköová, P. Veteška, Ľ. Bača, and J. Híveš, “Surface characterisation and wettability of titanium diboride by aluminium at low temperature,” *Adv. Appl. Ceram.*, vol. 119, no. 1, pp. 22–28, (2020), doi: 10.1080/17436753.(2019).1687207.

[66] B. Basu, G. B. Raju, and A. K. Suri, “Processing and properties of monolithic TiB2 based materials,” *Int. Mater. Rev.*, vol. 51, no. 6, pp. 352–374, (2006), doi: 10.1179/174328006X102529.

[67] H. Li, J. Wu, Z. Yin, and H. Zhang, “Preparation and Applications of Mechanically Exfoliated Single-Layer and Multilayer MoS2 and WSe2 Nanosheets,” Account of chemical research, vol. 47, no. 4, pp. 1067–1075, (2014).

[68] J. Shen et al., “Liquid Phase Exfoliation of Two-Dimensional Materials by Directly Probing and Matching Surface Tension Components,” Nano Letters, vol. 15, no. 8, pp. 5449–5454, (2015).

[69] G. Cunningham et al., “Solvent Exfoliation of Transition Metal Dichalcogenides: Dispersibility of Exfoliated Nanosheets Varies Only Weakly between Compounds,” ACS Nano, vol. 6, no. 4, pp. 3468–3480, (2012).

[70] R. Patidar, H. Gunda, A. K Varma, R. Gawas, S.K Das, K. Jasuja, Co-solvent exfoliation of layered titanium diboride into few-layer-thick nanosheets. Ceram Int[Internet].(2020);(May):0–1.Availablefrom: https://doi.org/10.1016/j.ceramint.(2020).07.336

[71] R. K. · A. R. · M. R. · S. J. · R. J. · M. A. Akram, "TiO2@NbSe2 decorated nanocomposites for efficient visible-light photocatalysis," *Eur. Biophys. J.*, no. September (2019), pp. 1–22, (2016).

[72] C. F. Holder and R. E. Schaak, "Tutorial on Powder X-ray Diffraction for Characterizing Nanoscale Materials," *ACS Nano*, vol. 13, no. 7, pp. 7359–7365, (2019), doi: 10.1021/acsnano.9b05157.

[73] M. Z. Khan, I. H. Gul, M. M. Baig, and A. N. Khan, "Comprehensive study on structural, electrical, magnetic and photocatalytic degradation properties of Al3+ ion," *J. Alloys Compd.*, vol. 848, p. 155795, (2020), doi: 10.1016/j.jallcom. (2020).155795.